University of Utrecht

Debye Institute
Nanophotonics Group

Interaction and polarization measurements of photon Bose-Einstein condensate

Author:
Fons van der Laan B.Sc.

Supervisors:
Sebastiaan Greveling M.Sc.
Dr. Dries van Oosten

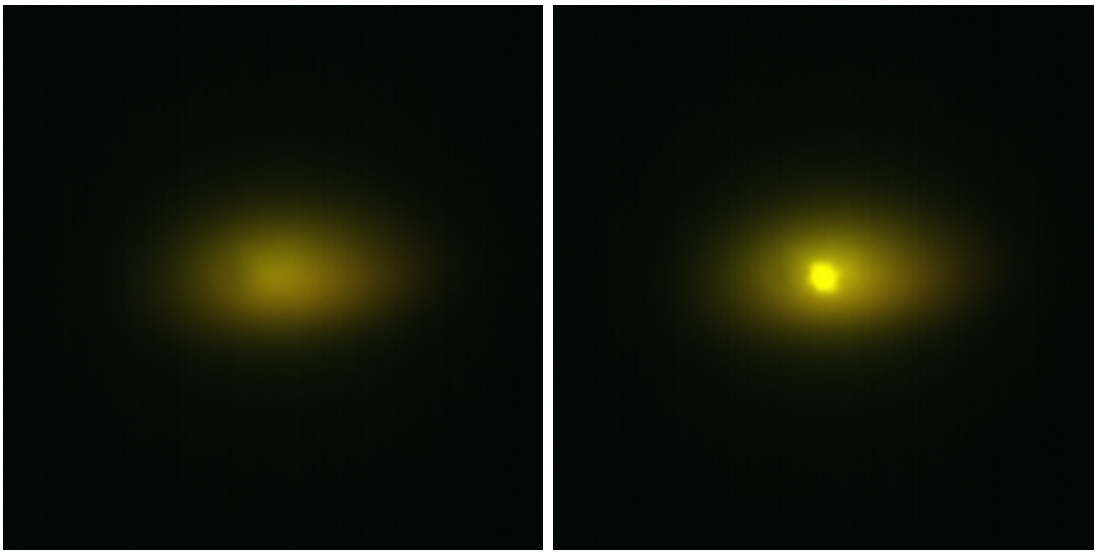

July 31, 2017

Abstract

Bose-Einstein condensation (BEC) is a state of matter where bosons macroscopically occupy the ground state of a system. In 2010 the group of Martin Weitz achieved a two-dimensional Bose-Einstein condensation of photons by using a dye-filled microcavity [1]. In 2015 our research group also achieved a photon BEC using a similar setup [2]. Although one expects the photons to be non-interacting, the radius of the condensate has been shown to grow as a function of photon density. This implies repulse photon-photon interactions. This leads us to question what the strength of the interactions is.

To investigate the interaction strength we take single shot images of the photon gas, while varying the photon density in the cavity. From each image we determine the number of condensate photons and the radius of the condensate. Subsequently we determine the interaction strength to be $\tilde{g} = (6.6 \pm 0.7) \times 10^{-3}$ and $\tilde{g} = (8 \pm 1) \times 10^{-2}$ using a dye concentration of 1.5 mM and 6.0 mM respectively. This implies that the interaction strength increases for increasing dye concentration. The source of the interactions is not yet understood and should be investigated further.

We also determine the polarization state of the photon gas. In order to do so we build an experimental setup which can measure all four Stokes parameters simultaneously. Since the phase transition into Bose-Einstein condensation is an example of spontaneous symmetry breaking, one would expect the condensate to have a different polarization each time it is created. We show that this is not the case and that every newly created BEC has the same polarization state, i.e. linearly polarized in the horizontal direction. We show this symmetry breaking is not affected by the dye concentration, photon density inside the cavity or the cavity mirrors. It is however caused by the intra-cavity polarization of the pump beam. We show that we can rotate the direction of the polarization by rotating the intra-cavity polarization of the pump beam.

Contents

1. Introduction

Bose-Einstein condensation (BEC) has become a very popular research field among physicist since it was experimentally achieved two decades ago [3, 4]. The theoretical foundation was proposed for photons by Bose in 1924 [5] and generalized for atoms by Einstein in 1925 [6]. A well-known photon gas in equilibrium is black body radiation [7]. Bose described an alternative derivation of black body radiation where he used a new way to count quantum states of photons. Einstein generalized this to massive bosons. Their work resulted in the concept of Bose-Einstein statistics, which describes particles with integer spin (bosons). The key feature of bosons is that they do not follow the Pauli exclusion principle, making it possible for them to share the same quantum state. Bose and Einstein predicted that massive bosons obeying these statistics would, under certain conditions, develop a macroscopic occupation of the groundstate. This is what is now called a Bose-Einstein condensate.

In order to achieve BEC one has to, independently of each other, control the temperature and the number of particles in the system. For atoms, several experimental cooling and trapping techniques had to be developed in other achieve sufficient low temperatures for BEC to occur [3,8,9]. For black body radiation there exists a relation between the temperature and the photon number. If the temperature changes, the number of photons is also affected. Therefore the number of photon is not conserved. Hence the experimental focus lay on atomic BEC and other massive particles [10–12].

In 2010 the group of Martin Weitz achieved a Bose-Einstein condensate of photons [1]. They were able to decouple temperature and photon number by placing the photons in a dye-filled microcavity consisting of two highly reflecting curved mirrors. The cavity induces a harmonic potential and an effective mass for the photons. This creates a two-dimensional trapped photon gas with a ground state in the center of the cavity. The dye causes the photon gas to thermalize via multiple absorption and emission cycles. The photon gas consequently takes on the temperature of the dye. The photon number in the cavity is determined by the power of the laser used to pump light into the cavity. Consequently they found a method to tune the number of photons independently of the temperature while keeping the photon number conserved. When the number of photons exceeds the cricital number a second order phase transition into Bose-Einstein condensation is observed.

As of 2015 we became the third research group to achieve Bose-Einstein condensation of photons [2]. For this we also use a dye-filled microcavity where we inject the photons using a pump laser. The phase transition caused by pumping beyond the critical photon number is shown in Figure 1.1. The left panel shows a two-dimensional

photon gas in equilibrium below threshold. In the right panel the number of photons is increased beyond threshold and a bright Bose-Einstein condensate is formed in the center of the cavity. A lot of properties of a photon BEC are still open questions. The first of which is if there are photon-photon interactions present in the condensate. Given that we describe the photons in the cavity as an ideal Bose gas, we would expect no interactions to be present. However the radius of the condensate has been shown to grow as a function of condensate fraction [1, 2]. This implies repulsive photon-photon interactions. The question then becomes what the interaction strength is. One can also wonder what the polarization state of the BEC is and more importantly if it changes for every newly created BEC. In this thesis we shall describe how we determine the answers to these questions.

In Section 2 we describe the theory behind our setup and Bose-Einstein condensation of photons in general. The theoretical description of polarization is also reviewed in this Section. Details of our experimental setup are discussed in Section 3. We present the results in Sections 4 and 5. Finally we end with a conclusion and discussion in Section 6.

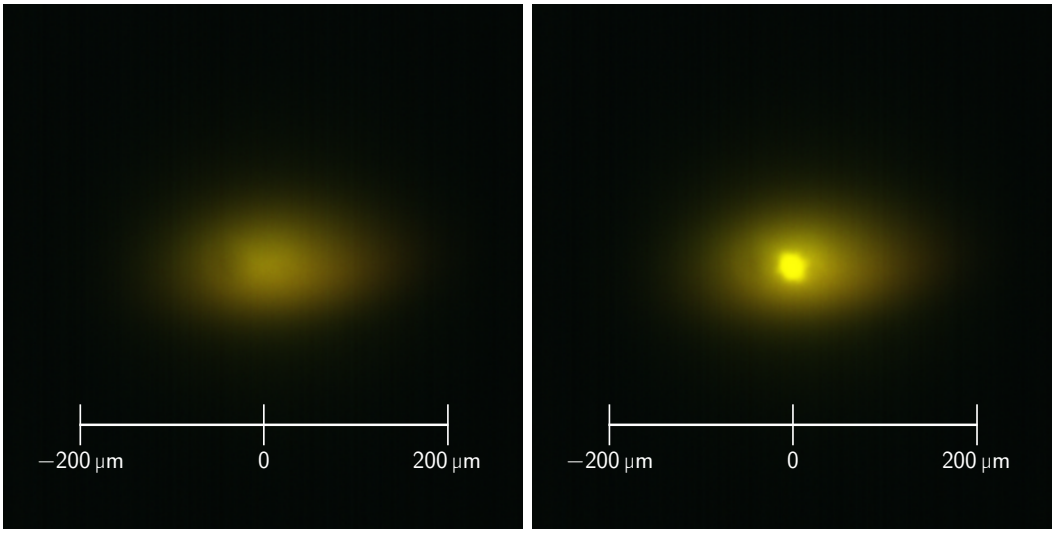

Figure 1.1: Left: A two-dimensional photon gas in thermal equilibrium below threshold. Right: When pumped beyond the critical number a Bose-Einstein condensate is formed in the center of the cavity.

2. Theory

Photon Bose-Einstein condensation in a dye-filled microcavity

In order to obtain Bose-Einstein condensation in two dimensions one needs the system to have a trapping potential with a ground state, a process to thermalize and number conservation. The system that we use to obtain Bose-Einstein condensation is a dye-filled microcavity. The microcavity consists of two highly reflecting curved mirrors. The photons inside the cavity thermalize via the dye molecules through multiple absorption and emission cycles [2, 13]. The rest energy of the photon is much larger than the thermal energy, thus on average no thermal photons are created or annihiliated. Thereby average number conservation is ensured [2, 13]. The theory for this is already discussed in previous work [2] and shall therefore not be repeated here. Here we will only discuss the trapping potential, Bose-Einstein statistics, the length scale of the Bose-Einstein condensate and interactions in the condensate.

Trapping potential

To understand how the curved cavity mirrors induce a trapping potential for the photons inside it, we look at the dispersion relation of the light inside the cavity. We write the energy of the photons in terms of the absolute value of the wave vector $\mathbf{k}$. Because of the symmetry of the system, we decompose $|\mathbf{k}|$ into longitudinal wavenumber k_z and transversal wavenumber $k_r = \sqrt{k_x^2 + k_y^2}$. That way the energy is written as

$$E_{\mathrm{ph}} = \frac{\hbar\, c}{n}\sqrt{k_z^2 + k_r^2}, \tag{2.1}$$

where $\hbar$ is the reduced Plancks constant, c is the speed of light and n is the refractive index of the dye solvent. Because the distance between the mirrors is in the order of the wavelength, only one longitudinal wavenumber is allowed, making k_z depend on the distance from the center $r = |\mathbf{r}|$. If we take the boundary conditions at the mirrors into account, we know that half the wavelength must fit an integer multiple times between the mirrors, i.e.

$$k_z(r) = \frac{q\,\pi}{D(r)} \qquad \text{with } q \in \mathbb{N}, \tag{2.2}$$

where q is the longitudinal mode number and $D(r)$ is the distance between the mirrors as a function of r. The distance can be written as

$$D(r) = D_0 - 2\left(R - \sqrt{R^2 - r^2}\right), \tag{2.3}$$

where R denotes the radius of curvature of the cavity mirrors and $D_0 = D(0)$. We now use the paraxial approximation, meaning $k_r \ll k_z$ and $r \ll R$. We also split the refractive index into the linear part n_0 and non-linear part n_2. Applying this and assuming the non-linear part of the refractive index to be negligible, the photon energy can be written as [2, 13]

$$E_{\mathrm{ph}}(\mathbf{r}, k_r) \approx m_{\mathrm{ph}} \left(\frac{c}{n_0}\right)^2 + \frac{(\hbar\, k_r)^2}{2\, m_{\mathrm{ph}}} + \frac{m_{\mathrm{ph}}\, \Omega^2}{2} r^2, \tag{2.4}$$

with the effective photon mass

$$m_{\mathrm{ph}} = \frac{\hbar}{(c/n_0)}\, k_z(0) = \frac{\hbar}{(c/n_0)}\, \frac{q\, \pi}{D_0}, \tag{2.5}$$

and the trapping frequency

$$\Omega = \left(\frac{c}{n_0}\right) \frac{1}{\sqrt{D_0\, R/2}}. \tag{2.6}$$

We recognize this as the energy of a non-relativistic massive particle in a harmonic potential. This is understand by looking at the longitudinal wavenumber. Since half the wavelength must fit an integer times between the cavity mirrors, the longitudinal wavenumber of photons existing more radially outwards must be larger. Therefore their energy becomes larger when going outwards, which causes the trap. Because their longitudinal wavenumber is no longer free, the photons gas effectively becomes two-dimensional. Therefore we establish a trapped two-dimensional photon gas.

Bose-Einstein statistics

A two-dimensional harmonic oscillator can be written in terms of two one-dimensional harmonic oscillators. The eigenfunctions become the product of the two one-dimensional eigenfunctions. The energy is a sum of the two and is therefore given by [14]

$$\varepsilon_n = \hbar\, \Omega_x\, (n_x + \frac{1}{2}) + \hbar\, \Omega_y\, (n_x + \frac{1}{2}) = \hbar\Omega(n+1), \tag{2.7}$$

where n is the principal quantum number of the two-dimensional harmonic oscillator. We know that $\Omega = \Omega_x = \Omega_y$ since the harmonic potential is isotropic. Since the energy only depends on n, the degeneracy $g(\varepsilon_n)$ is given by the number of ways you can add op n_x and n_y to get n, i.e. $g(\varepsilon_n) = N_s(n+1)$. Here N_s denotes the degeneracy due to the polarization degeneracy of the photons.

As photons are bosons with a non-interacting nature, their statistics can be described as an ideal Bose gas. Since the photons are trapped in a harmonic potential, the photon energy is discrete. Therefore the expected number of photons with energy ε_n is given by the degeneracy mutiplied by the Bose-Einstein distribution

$$n(\mu, T, \varepsilon_n) = \frac{g(\varepsilon_n)}{e^{(\varepsilon_n - \mu)/k_\mathrm{B}T} - 1}, \tag{2.8}$$

where μ is the chemical potential, k_B the Boltzmann constant and T the temperature. Here we need to discuss the role of temperature. Temperature is a property described in an ensemble. In our case the ensemble is a photon gas, which has a well defined temperature, which we call the spectral temperature. We expect the spectral temperature to be equal to the temperature of the dye molecules, but this is very challenging to check experimentally. We will however determine the temperature using a fit routine as we describe at the end of this Section.
For the total number of photons in the system, we sum over all energies

$$N = \sum_{\varepsilon_n} \frac{g(\varepsilon_n)}{e^{(\varepsilon_n - \mu)/k_\mathrm{B}T} - 1}. \tag{2.9}$$

We compare $\hbar\Omega$ with $k_\mathrm{B}T$ using typical values of $R = 1\,\mathrm{m}$, $n_0 = 1.43$, and $D_0 = 1.5\,\mu\mathrm{m}$. We see that $k_\mathrm{B}T$ is much larger than $\hbar\Omega$. We therefore can use ε_n and n as continuous variables. This also changes the degeneracy $g(\varepsilon_n)$ into a density of states $\mathcal{D}(\varepsilon)$. Calculating $\mathcal{D}(\varepsilon)$ is done by first looking at the number of states $\mathcal{N}(\varepsilon)$ with energies up to ε given by [2]

$$\mathcal{N}(\varepsilon) = \frac{N_s}{2} \left(\frac{\varepsilon}{\hbar\,\Omega}\right)^2. \tag{2.10}$$

The density of states is defined as [15]

$$\mathcal{D}(\varepsilon) = \frac{\mathrm{d}\mathcal{N}(\varepsilon)}{\mathrm{d}\varepsilon} = N_s \frac{\varepsilon}{\hbar^2\,\Omega^2}. \tag{2.11}$$

The expected number of photons with energy ε is now found by multiplying the density of states with the Bose-Einstein distribution

$$n(\mu, T, \varepsilon) = \frac{\mathcal{D}(\varepsilon)}{e^{(\varepsilon_n - \mu)/k_\mathrm{B}T} - 1} = N_s \frac{\varepsilon}{\hbar^2\,\Omega^2} \frac{1}{e^{(\varepsilon_n - \mu)/k_\mathrm{B}T} - 1}. \tag{2.12}$$

To obtain the total number of photons in the system we now integrate over the energy

$$N = N_s \int_0^\infty \frac{\varepsilon}{\hbar^2\,\Omega^2} \frac{1}{e^{(\varepsilon_n - \mu)/k_\mathrm{B}T} - 1} \mathrm{d}\varepsilon. \tag{2.13}$$

The critical photon number N_c is calculated by evaluating this integral for $\mu = 0$, which gives the relation between N_c and T

$$N_c = N_s \frac{\pi^2}{6} \left(\frac{k_\mathrm{B}T}{\hbar\Omega}\right)^2. \tag{2.14}$$

When the number of photons in the system exceeds N_c a Bose-Einstein condensate is created. In cold atom physics one usually looks at a critical temperature T_c under which a Bose-Einstein condensate will form. This is done because they lower the temperature to achieve BEC. For us it is experimentally difficult to lower the temperature, but it is simple to increase the number of photon above N_c by increasing the power of our pump laser.

Length scale of the system

The Bose-Einstein condensate is the macroscopic occupation of the ground stated. In order to determine growth in size of the condensate we look at the size of the ground state of the system. In a harmonic oscillator the size of the ground state is described by the harmonic oscillator length [14]

$$l_{\mathrm{HO}} = \sqrt{\frac{\hbar}{m_{\mathrm{ph}}\Omega}}. \tag{2.15}$$

We would like to write l_{HO} in terms of parameters we can measure. To do this we must first rewrite m_{ph} and Ω from Equations (2.5) and (2.6). Both contain the distance between the cavity mirrors in the middle of the cavity D_0. From Equation 2.2 we know that $D_0 = q\,\lambda_{\mathrm{cutoff}}/2\,n_0$, where $\lambda_{\mathrm{cutoff}}$ is measured in a spectrometer and related to the longitudinal wavenumber as $\lambda_{\mathrm{cutoff}} = 2\,\pi\,n_0/k_z(0)$. Using this we can write m_{ph} and Ω as

$$m_{\mathrm{ph}} = \frac{2\,\pi\,\hbar}{(c/n_0)\,(\lambda_{\mathrm{cutoff}}/n_0)} \quad \text{and} \quad \Omega = \frac{c}{n_0}\,\frac{2}{\sqrt{q\,R\,(\lambda_{\mathrm{cutoff}}/n_0)}}. \tag{2.16}$$

If we insert these into Equation 2.15 we obtain

$$l_{\mathrm{HO}} = \sqrt{\frac{1}{4\,\pi}\,\frac{\lambda_{\mathrm{cutoff}}}{n_0}}\,\sqrt[4]{q\,R\,\frac{\lambda_{\mathrm{cutoff}}}{n_0}}. \tag{2.17}$$

Note that by $\lambda_{\mathrm{cutoff}}$ we mean the vacuum wavelength of the light as measured in the spectrometer. The wavelength in the cavity is then given by $\lambda_{\mathrm{cutoff}}/n_0$. The advantage of expressing l_{HO} in terms of $\lambda_{\mathrm{cutoff}}$ and q is that $\lambda_{\mathrm{cutoff}}$ can be measured using a spectrometer and q can be calculated from the free spectral range. The free spectral range $\Delta\omega$ is given by [16]

$$\Delta\omega = \frac{\pi\,c}{n_0\,D_0}. \tag{2.18}$$

We fill in D_0 and rewrite to get

$$q = \frac{2\,\pi\,c}{\lambda_1\,\Delta\omega}. \tag{2.19}$$

Using $\omega = 2\,\pi\,c/\lambda$ we write

$$\Delta\omega = \frac{2\,\pi\,c(\lambda_1 - \lambda_2)}{\lambda_1\,\lambda_2}, \tag{2.20}$$

Where λ_1 and λ_2 denote the wavelengths of the adjacent peaks in the spectrum. Finally we get an expression for q

$$q = \frac{\lambda_1}{\lambda_1 - \lambda_2}. \tag{2.21}$$

Density distribution of photons

We describe the photons inside the cavity using well-known eigenmodes of the harmonic potential. The wavefunctions are written as a product of two one dimensional harmonic oscillator wavefunctions ψ_{n_x} and ψ_{n_y}. We write the density $\rho(x, y)$ in terms of these eigenmodes and Bose-Einstein distribution.

$$\rho(x,y) = \sum_{n_x,n_y} \frac{1}{e^{(\varepsilon_n - \mu)/k_B T} - 1} |\psi_{n_x}(x)\psi_{n_y}(y)|^2 \qquad \text{with } n = n_x + n_y. \tag{2.22}$$

Note that $g(\varepsilon_n)$ is not included in this sum since the sum is over all n_x and n_y and not over the principal quantum number n or all energies ε_n. The downside of this expression is that it contains a double sum. We can however use the restriction that $n_x + n_y = n$. Therefore we rewrite it into

$$\rho(x,y) = \sum_{n} \frac{g(\varepsilon_n)}{e^{(\varepsilon_n - \mu)/k_B T} - 1} \rho_n(x,y), \tag{2.23}$$

where $\rho_n(x, y)$ is the average density profile of all states with principal quantum number n

$$\rho_n(x,y) = \frac{1}{n+1} \sum_{n_x=0}^{n} |\psi_{n_x}(x)\psi_{n_y}(y)|^2 = \frac{1}{n+1} \sum_{n_x=0}^{n} |\psi_{n_x}(x)\psi_{n-n_x}(y)|^2. \tag{2.24}$$

Since the system is radially symmetric, we know that $\rho_n(x, y)$ can only depend on r, the distance from the center of the trap. We therefore radially average $\rho_n(x, y)$ into $\rho_n(r)$ and obtain

$$\rho(r) = \sum_{n} \frac{g(\varepsilon_n)}{e^{(\varepsilon_n - \mu)/k_B T} - 1} \rho_n(r). \tag{2.25}$$

The great advantage of this is that $\rho_n(r)$ does not depend on the chemical potential or temperature. It does however depend on l_{HO} and Ω. Since they depend on the cavity distance, it is difficult to exactly know them before the experiment. To counter this problem we express r in units of l_{HO} and μ and T in units of $\hbar\Omega$. This makes

the $\rho_n(r)$ dimensionless. Therefore the functions $\rho_n(r)$ can be precomputed and do not need to be calculated during a fitting procedure.

As an illustration Figure 2.1 shows multiple theoretical density profiles where μ is increased from below threshold to above threshold, while the temperature is kept constant at 300 K. Each curve is given an artificial offset to be able to distinguish them. The curves are produced using $l_{\mathrm{HO}} = 7.5\,\mu\mathrm{m}$ and $\Omega = 2 \times 10^{11}\,\mathrm{Hz}$. The density profiles are plotted on a logarithmic scale to better see the features in the profiles. All density profiles show a thermal cloud extending to $\sim 300\,\mu\mathrm{m}$. When μ is increased a peak forms on top of the thermal cloud at $r = 0$. This peak is the Bose-Einstein condensate. Moving away from the center a steep drop is shown because of the finite size of the condensate. After this the density profile is linear.

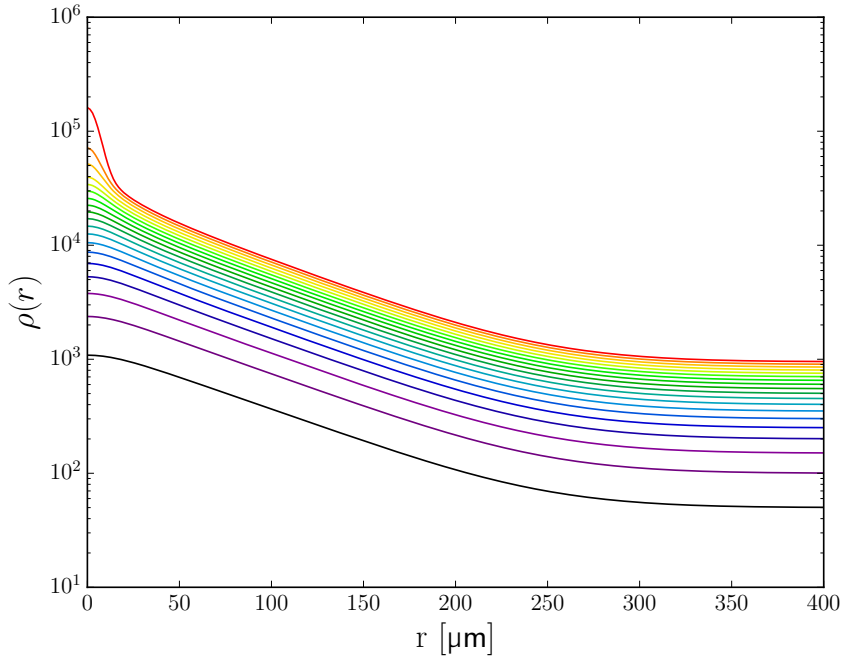

Figure 2.1: Density profiles, where μ is increased from below threshold to above it.

Interactions in a photon Bose-Einstein condensate

Typically photons are known for their non-interactive nature. However, in early experiments a growth in size of the condensate is observed when increasing the photon number [1]. This signals repulsive interactions in the condensate. The repulsive interactions make it more energetically favourable to increase the interparticle distance. Although the origin of these interactions is still unknown, a theoretical model is developed by Van der Wurff et. al. [17]. The theory uses second quantization to look

at the grand potential of the photon gas $V_{\mathrm{gr}}[\phi_0]$, where ϕ_0 is the macroscopic wave function of the Bose-Einstein condensate. Note here that this is not related to the trapping frequency as discussed earlier. They assume the interaction to be a contact interaction, creating the following energy functional

$$V_{\mathrm{gr}}[\phi_0] = \int \mathrm{d}\mathbf{x} \left[\frac{\hbar}{2m_{\mathrm{ph}}} |\nabla\phi_0(\mathbf{x})|^2 + \left(V(\mathbf{x}) - \mu + \frac{g}{2}|\phi_0(\mathbf{x})|^2 \right) |\phi_0(\mathbf{x})|^2 \right]. \tag{2.26}$$

Here $\mathbf{x}$ denotes the two-dimensional position, $V(\mathbf{x})$ the harmonic trapping potential, μ the chemical potential and g is introduced as the coupling constant of the effective pointlike interaction between the photons. As can be seem from the energy functional, the coupling constant is not a operator acting on ϕ_0, but simply a constant. They then use the Bogoliubov substitution to write $\phi_0(\mathbf{x})$ as normalized variational wavefunction $\psi_q(\mathbf{x})$. They assume the kinetic energy to be large compared to the interaction energy and thus the variational wavefunction to be Gaussian, i.e.

$$\psi_q(\mathbf{x}) = \frac{1}{\sqrt{\pi}\, q} e^{-|\mathbf{x}|^2/2q^2}, \tag{2.27}$$

where q is the width of the Gaussian and not the longitudinal mode number. This is a good approximation if the interaction is weak, which is reasonable given that we are use to photons not interacting at all. Subsequently they substitute this into the energy functional and minimize it with respect to the variational parameter q, leading to

$$q_{\mathrm{min}} = \sqrt[4]{\frac{2\,\pi\,\hbar^2 + m_{\mathrm{ph}}\, N_0\, g}{2\,\pi\,\Omega^2\, m_{\mathrm{ph}}^2}} = l_{\mathrm{HO}} \sqrt[4]{1 + \frac{\tilde{g}\, N_0}{2\,\pi}}, \tag{2.28}$$

where N_0 denotes the number of photons in the condensate and $\tilde{g} = m_{\mathrm{ph}}\, g/\hbar$ the dimensionless coupling constant. We will use $\tilde{g}$ as the interaction strength. The assumption that the wavefunctions are Gaussian is valid for a small number of condensate photons, i.e. $\tilde{g}\, N_o/2\,\pi \ll 1$. There is also the limit where the kinetic energy is negligible with respect to the interaction energy. This is called the Thomas-Fermi limit [18]. Thus when $\tilde{g}\, N_o/2\,\pi$ gets to large, the Thomas-Fermi limit is more appropiate. This is either due to a large interaction strength or a large number of condensate photons.

Polarization

Polarization is a property of light, which can be best explained if we look at light as a electromagnetic wave. The electric and magnetic fields of an electromagnetic wave are perpendicular to each other and transverse to the direction of propagation. Convention is to define the z-axis as the axis of propagation and the x- and y-axis aligned to the electric field and magnetic field respectively [19]. The polarization of

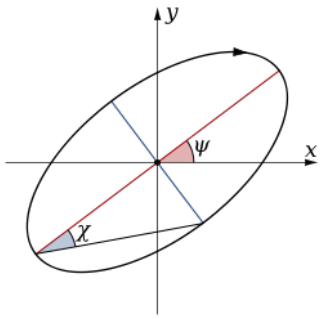

Figure 2.2: The electric field vector forms a ellipse when projected in the x-y plane. The ellipse is described by the orientation angle ψ and ellipticity angle χ.

the electromagnetic wave is defined as the direction of the electric field. The electric and magnetic fields are described as

$$\mathbf{E}(\mathbf{r},t) = \begin{pmatrix} E_{0,x}\cos(kz-\omega t) \\ E_{0,y}\cos(kz-\omega t+\delta) \\ 0 \end{pmatrix}, \tag{2.29}$$

$$\mathbf{B}(\mathbf{r},t) = \frac{1}{c}\begin{pmatrix} -E_{0,y}\cos(kz-\omega t+\delta) \\ E_{0,x}\cos(kz-\omega t) \\ 0 \end{pmatrix}, \tag{2.30}$$

where c is the speed of light, k is the wavenumber, ω is the angular frequency and δ the phase difference between the amplitudes in x- and y-direction.

If $\delta = 0$, the plane of the electric field does not change as the wave propagates. The wave is then called linearly polarized. If $\delta = \pm\pi/2$ the electric field vector describes a circle if projected on the x-y plane. The wave is called circularly polarized. In that case the absolute value of the electric field vector never becomes zero but circles around the z-axis. Depending on the sign of the phase difference a circularly polarized wave is called left-handed or right-handed polarised.

All other cases are a combination of the former two and are called elliptically polarised. One could also say that the linear and circularly polarised light are a special case of elliptically polarised light. The polarisation of the wave can be described by a so-called polarization ellipse as shown in Figure 2.2. The ellipse is determined by the orientation angle ψ, defined as the angle between the major axis of the ellipse and the x-axis, and the ellipticity angle χ, defined by the arctan of the ration between the minor and major axis of the ellipse.

Although ψ and χ, together with the handedness of the ellipse, describe the polarization state of the light, the disadvantages of them are that they cannot described random polarization and cannot be measured directly.

Stokes parameters

Another way to describe the polarization state of light are the so-called Stokes parameters. George Gabriel Stokes defined these as a way to describe the polarization in terms of intensity instead of field vectors. The main advantage of this is that intensity can be measured. In order to do so he needed four parameters [20];

$$S_0 = I_{\text{tot}}, \tag{2.31}$$
$$S_1 = I_{0^\circ} - I_{90^\circ}, \tag{2.32}$$
$$S_2 = I_{45^\circ} - I_{-45^\circ}, \tag{2.33}$$
$$S_3 = I_{\text{LHC}} - I_{\text{RHC}}, \tag{2.34}$$

where I_{tot} is the total intensity of the light. The rest of the subscripts denote the angle of the horizontal polarization of the light or stand for left-handed circular of right-handed circular light. The Stokes parameters make use of the fact that linearly polarized light can be projected onto an orthogonal basis. The same holds for circular polarized light. All Stokes parameters can have a value between -1 and 1. If for example $S_1 = 1$ this indicates that the light is horizontally polarized. If $S_1 = -1$, the light is vertically polarized. If S_1 takes on a value in between the polarization (projected on the $0^\circ/90^\circ$ basis) is a superposition of both. With these four parameters the polarization state of the light can be fully described.

A different way of defining the Stokes parameters is shown below [20];

$$S_0 = I_{\text{tot}}, \tag{2.35}$$
$$S_1 = I_{\text{tot}}\, p\, \cos(2\psi)\, \cos(2\chi), \tag{2.36}$$
$$S_2 = I_{\text{tot}}\, p\, \sin(2\psi)\, \cos(2\chi), \tag{2.37}$$
$$S_3 = I_{\text{tot}}\, p\, \sin(2\chi), \tag{2.38}$$

where p is the degree of polarization and ψ and χ are the parameters of the polarization ellipse as described earlier.

Stokes parameters are often normalized to the intensity, such that S_0 becomes 1, since the polarization is independent of the intensity. From here on, when we talk about Stokes parameters, we will these mean normalized Stokes parameters.

In both descriptions the squared sum of the last three Stokes parameters yields the degree of polarization

$$p = \sqrt{S_1^2 + S_2^2 + S_3^2}. \tag{2.39}$$

Stokes Vector

In order to work with Stokes parameters they are often combined into a vector, called the Stokes vector, which is defined as

$$\mathbf{S} = \begin{pmatrix} S_0 \\ S_1 \\ S_2 \\ S_3 \end{pmatrix}. \tag{2.40}$$

From this we can easily work with different polarization states. For example, linear 0° polarised light is described by

$$\mathbf{S}_{0^\circ} = \begin{pmatrix} 1 \\ 1 \\ 0 \\ 0 \end{pmatrix}, \tag{2.41}$$

and left-handed circular light by

$$\mathbf{S}_{\text{LHC}} = \begin{pmatrix} 1 \\ 0 \\ 0 \\ -1 \end{pmatrix}. \tag{2.42}$$

One of the advantages of using a Stokes vector is that the effects of optical elements on the polarization state can be described in linear algebra using a matrix. These matrices are called Mueller matrices. A common optical element is a linear polariser. Its matrix is given by [21]

$$\frac{1}{2}\begin{pmatrix} 1 & \cos(2\theta) & \sin(2\theta) & 0 \\ \cos(2\theta) & \cos^2(2\theta) & \sin(2\theta)\cos(2\theta) & 0 \\ \sin(2\theta) & \sin(2\theta)\cos(2\theta) & \sin^2(2\theta) & 0 \\ 0 & 0 & 0 & 0 \end{pmatrix}, \tag{2.43}$$

where θ is the angle that the transmission axis of the polarizer makes with the x-axis. For a linear polarizer with horizontal transmission, i.e. $\theta = 0$, this matrix reduces to

$$\frac{1}{2}\begin{pmatrix} 1 & 1 & 0 & 0 \\ 1 & 1 & 0 & 0 \\ 0 & 0 & 0 & 0 \\ 0 & 0 & 0 & 0 \end{pmatrix}. \tag{2.44}$$

When this matrix is applied to $\mathbf{S}_{0^\circ}$ it indeed filters horizontal polarized light, as shown in Equation 2.45.

$$\frac{1}{2}\begin{pmatrix} 1 & 1 & 0 & 0 \\ 1 & 1 & 0 & 0 \\ 0 & 0 & 0 & 0 \\ 0 & 0 & 0 & 0 \end{pmatrix}\begin{pmatrix} 1 \\ 1 \\ 0 \\ 0 \end{pmatrix} = \begin{pmatrix} 1 \\ 1 \\ 0 \\ 0 \end{pmatrix} \tag{2.45}$$

If the matrix is applied to $\mathbf{S}_{\text{LHC}}$, the outgoing light is horizontally polarized, but its intensity is half.

More interesting optical elements, when it comes to polarization, are retarders. The propagation of the electromagnetic field in these retarders is different for different polarizations. This causes one polarization to get retarted, delayed, with respect to the other. The phase difference changes the polarization of the outgoing light. There are two special cases where the retarders are interesting; a phase shift of π, half an optical cycle and a phase shift of $\pi/2$, a quarter optical cycle. For this reason these retarders are called a half waveplate and a quarter waveplate. This can also be seen in the property of waveplates, which is called retardance. A half waveplate has a retardance of 0.5 and a quarter waveplate a retardance of 0.25. The retardance of a waveplate is equal to $2\pi/\delta$, where δ is the phase difference between the fast and the slow axis. In general the matrix for waveplates is given by [20]

$$\begin{pmatrix} 1 & 0 & 0 & 0 \\ 0 & \cos^2(2\theta) + \cos(\delta)\sin^2(2\theta) & \cos(2\theta)\sin(2\theta) - \cos(\delta)\cos(2\theta)\sin(2\theta) & \sin(\delta)\sin(2\theta) \\ 0 & \cos(2\theta)\sin(2\theta) - \cos(\delta)\cos(2\theta)\sin(2\theta) & \cos^2(2\theta) + \cos(\delta)\sin^2(2\theta) & -\sin(\delta)\cos(2\theta) \\ 0 & -\sin(\delta)\sin(2\theta) & \sin(\delta)\cos(2\theta) & \cos(\delta) \end{pmatrix},$$

where θ is the rotation of the fast axis of the waveplate and δ is the phase difference between the fast and slow axis. For a half waveplate, $\delta = \pi$, with the fast axis rotated to 45° the matrix reduces to

$$\begin{pmatrix} 1 & 0 & 0 & 0 \\ 0 & -1 & 0 & 0 \\ 0 & 0 & 1 & 0 \\ 0 & 0 & 0 & -1 \end{pmatrix}. \tag{2.46}$$

When this matrix is applied to $\mathbf{S}_{0°}$, it is transformed to $\mathbf{S}_{90°}$, as shown in Equation 2.47.

$$\begin{pmatrix} 1 & 0 & 0 & 0 \\ 0 & -1 & 0 & 0 \\ 0 & 0 & 1 & 0 \\ 0 & 0 & 0 & -1 \end{pmatrix} \begin{pmatrix} 1 \\ 1 \\ 0 \\ 0 \end{pmatrix} = \begin{pmatrix} 1 \\ -1 \\ 0 \\ 0 \end{pmatrix}. \tag{2.47}$$

Note that a waveplate does not change S_0, the intensity of the light, but only the other three Stokes parameters. This is not the case for linear polarisers.

One must know that the retardance of a waveplate is different for each wavelength, since the phase shift depends on the wavelength. Therefore most waveplates are made for a specific wavelength. There are also so-called achromatic waveplates, which have a nearly constant retardance for a range of wavelengths. For instance an achromatic half waveplate has a range of wavelengths for which the retardance is approximately the same, but it is not equal to 0.5. This causes the matrix to also have off-diagonal elements. Because of this the matrix mixes the incoming polarization state into a combination of linearly and circularly polarized light. Therefore it is important to accurately know the retardance of a waveplate.

Polarization of the Bose-Einstein condensate

The phase transition from below the critical number of photons in the system N_c to above it is an example of spontaneous symmetry breaking. The condensate chooses a well-defined polarization state, but as the system is symmetric, there is no preferred polarization state. Therefore we would expect the condensate to randomly choose a polarization state each time it is created. This is similar to a ferromagnetic system being cooled below the Curie temperature.

3. Experimental Setup

The experimental setup consists of two parts. The first is used to create Bose-Einstein condensation, measure the spectrum of it and capture the spatial distribution. This setup we call the BEC setup. The second setup is used to measure the polarization of the thermal cloud and the condensate. This we call the polarization setup. Here we describe both setups, starting with the BEC setup.

BEC Setup

A schematic overview of the BEC setup is shown in Figure 3.1. The main part of this setup is the dye-filled microcavity. The cavity consists of two mirrors (CRD Optics, 901-0010-0550) with a reflectivity of 99.9985 % and a radius of curvature of 1 m. The typical cavity length is 1.5 µm. In order to achieve this cavity length, one of the cavity mirrors is cut down to a cone. In this way the edges of the mirros do not touch for these short cavity distances. The cut down mirror has a remaining mirror surface with a diameter of 1.5 mm. Between the mirrors a droplet of rhodamine 6G, dissolved in ethylene glycol, is held in place using capillary forces. Before inserting the droplet, the mirror surfaces are cleaned with First Contact Polymer. To enable an accurate aligned cavity, the small cavity mirror is placed on a translation stage and the adjustment screws of the small cavity mirror mount are replaced by two piezo actuators.

The dye molecules inside the cavity are excited using a pump pulse from a CW laser (Laser Quantum Gem 532) with a wavelength of 532 nm. The pump pulse is created using 3 accousto optic modulators (AOM) in serie. The first AOM is used to accurately regulate the power of the pump light. This is done by applying a certain voltage to the AOM. The other two AOM's are used to created the pump pulse with an exctinction ratio of 5.4×10^4. This ensures that the leak light during the dark phase in the experiment is minimized. The pump beam is focused into the cavity under an angle of 65° with the optical axis of the cavity. We found a transmission maximum at this angle [2]. To further increase transmission the linear polarization of the pump beam is rotated to an optimum using a half waveplate.

In the translation stage a piezo element is placed to control the translation in the direction of the optical axis. The cavity length is locked using a feedback loop that controls this piezo element. To create the feedback signal a HeNe laser beam is directed into the cavity along the optical axis. Due to the curvature of the mirrors a

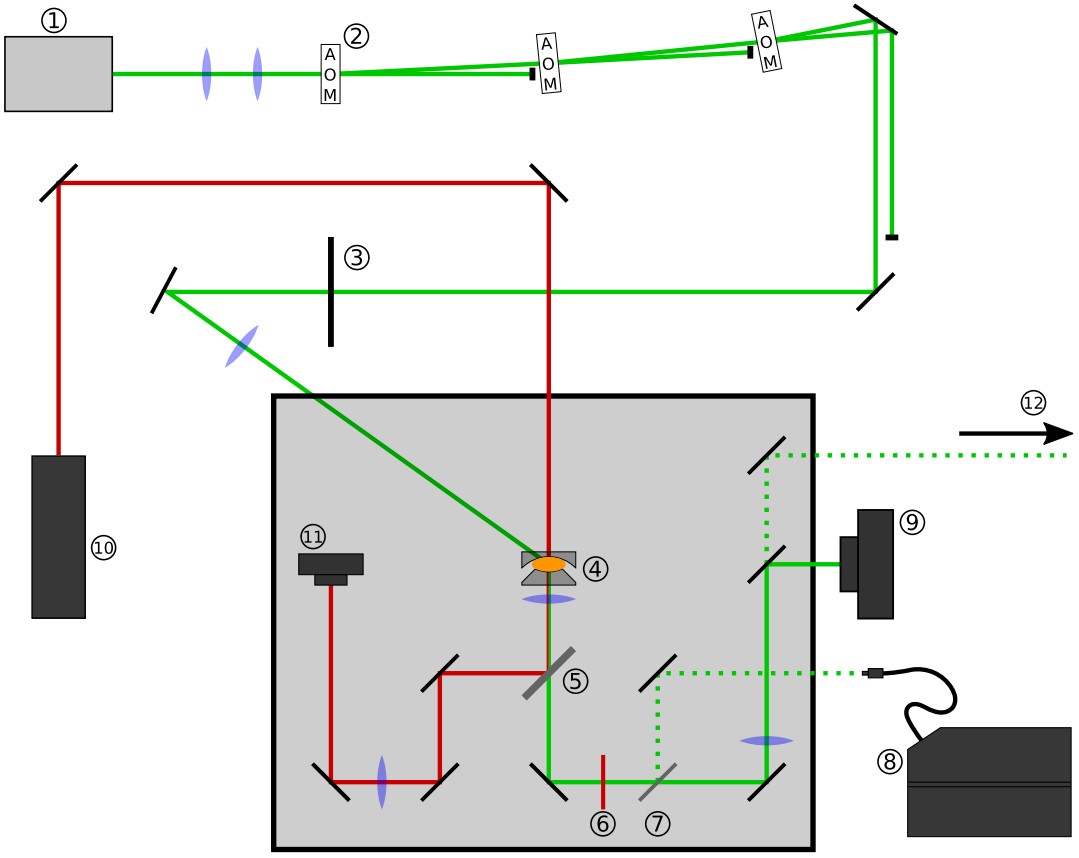

①	Pump laser with $\lambda = 532$ nm	⑦	45:55 Pellicle beamsplitter
②	AOM's to create pulse	⑧	Spectrometer
③	Half waveplate	⑨	Chameleon camera
④	Dye-filled microcavity	⑩	HeNe laser
⑤	Dichroic mirror at $\lambda = 635$ nm	⑪	Flea camera
⑥	Notch filter at $\lambda = 633$ nm	⑫	Towards polarization setup

Figure 3.1: Schematic overview of the setup used to create and image the Bose-Einstein condensate of light.

interference pattern of the HeNe laser light is formed. The interference pattern consist of thin rings, known as Newton rings [22]. The radius of these rings is determined by the cavity length. If the measured radius of the smallest ring differs from a set value, the piezo element will adjust the cavity length accordingly.

For the imaging of the condensate and locking of the cavity we use light that leaks through the cavity mirrors. The light is split into two paths; one used for imaging and one use for the cavity lock. To split the light we use a short pass dichroic mirror (Chroma ZT635dcrb) which reflects light with a wavelength of (635 ± 10) nm (cavity

lock) and transmits all other wavelengths (imaging). The light used for the cavity lock is directed to a fast monochrome camera (Point Grey Flea FL3-U3-13Y3M). Using the data from this camera we compute the radius of the inner Newton ring and regulate the cavity lock. The light used to image the Bose-Einstein condensate is also filtered using a notch filter. The notch filter filters out light with a wavelength of (633 ± 2) nm such that the HeNe laser is fully filtered out. Subsequently the light can be directed to a colour camera (Point Grey Chameleon, CMLN-13S2C-CS) used to capture the spatial distribution or it can be directed towards the polarization setup. When the light is directed to the Point Grey Chameleon a pellicle beamsplitter (45:55) can also be placed in the beam path to measure the spectrum.

Polarization setup

The setup to measure the polarization of the incoming light is placed after the BEC setup. A schematic overview is shown in Figure 3.2. The incoming beam first passes through two lenses to create an image on the camera (Andor Zyla 5.5). After which it is split into four different paths by three non-polarizing beam splitter cubes (BS). All the paths have the same length from the lens to the camera, such that we create four images on the camera simultaneously. The first path (red) functions as an unfiltered path and is directed to the camera without passing through any polarizers or waveplates. The second path (green) passes through a linear polarizer (Lin. Pol.) with its transmission axis placed at 0°. The third path (blue) also passes through a linear polarizer, but its transmission axis is placed at 45°. The last path (yellow) passes through a achromatic quarter lamba plate ($\lambda/4$) with its fast axis placed at 0° and a linear polarizer placed with its transmission axis at $-45°$. In this way the four paths correspond to the Stokes parameters discussed in Section 2.2.1.

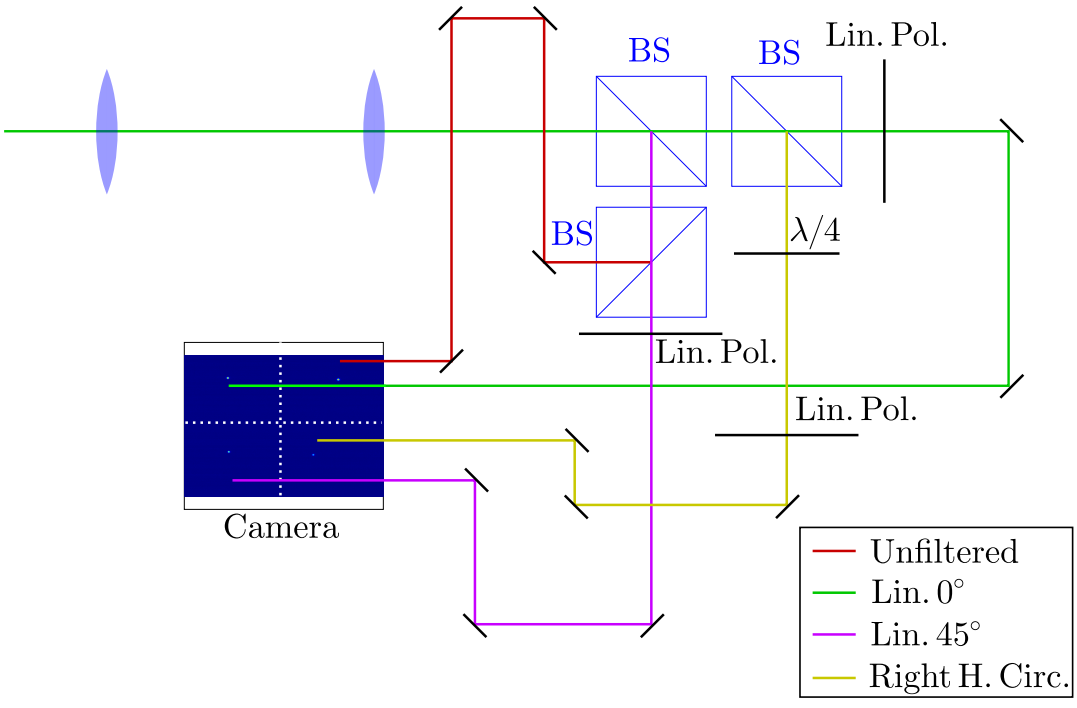

Figure 3.2: Schematic overview of the polarization setup.

Calibration

In order to reconstruct the polarization state of the condensate and the thermal cloud from a single camera image, we need to calibrate the polarization setup. The goal is to compute a matrix we can use to make a linear transformation from the camera image to a Stokes vector for every pixel. To do so we define a 4D vector consisting of 4 counts of our camera image. Using the Stokes vector as defined earlier, we could formally write our setup as one matrix $\overline{\mathbf{M}}$ which transform the Stokes vector $\mathbf{S}$ into a camera vector $\mathbf{C}$ as shown in Equation 3.2. This is justified because all effects due to optical elements can be seen as unitary transformations to the Stokes vector.

$$\overline{\mathbf{M}}\,\mathbf{S} = \mathbf{C} \tag{3.1}$$

$$\begin{pmatrix} m_{00} & \cdots & m_{03} \\ \vdots & \ddots & \vdots \\ m_{30} & \cdots & m_{33} \end{pmatrix} \begin{pmatrix} S_0 \\ S_1 \\ S_2 \\ S_3 \end{pmatrix} = \begin{pmatrix} \text{Unf} \\ \text{Lin. } 0^\circ \\ \text{Lin. } 45^\circ \\ \text{RHC} \end{pmatrix} \tag{3.2}$$

If we find this matrix $\overline{\mathbf{M}}$ and invert it, we could use this to transform our camera image back into a Stokes vector. In order to calibrate our setup, we thus need to find all matrix elements in $\overline{\mathbf{M}}$.

One of the advantages of computing this matrix is that we do not need to accurately know the effect of all optical elements in our polarization setup, since we are only interested in the combined matrix. Therefore we do not need to know the frequency or the angle dependence of every optical element in the setup, because this will be taken account into the final matrix.

In order to calibrate the setup, we do need to know the polarization state of the incoming light very accurately. We do this for multiple wavelengths since the Bose-Einstein condensate and thermal cloud consist of multiple wavelengths.

Calibration of waveplates

In order to know the polarization state of the incoming light we use a laser source and manipulate the light using multiple linear polarisers and waveplates. The advantages of a linear polarizer are that it is relatively simple, independent of wavelength and the polarization state of the outgoing light is well defined. This is not the case for waveplates since the retardance is wavelength dependent. If the retardance is not exactly π or $\pi/2$ it transfers the incoming light in a mixture a multiple different polarization states. Therefore it is essential that we very accurately know the retardance and the angle of the fast axis of the waveplates used to calibrate the polarization setup.

To compute the retardance we make sure we have linearly polarized light going through our waveplate. After the waveplate we placed a linear polarizer at 0° trans-

mission. We measure the light that is transmitted with a power meter. A schematic overview is shown in Figure 3.3, where the half waveplate is denoted by $\lambda/2$. Using

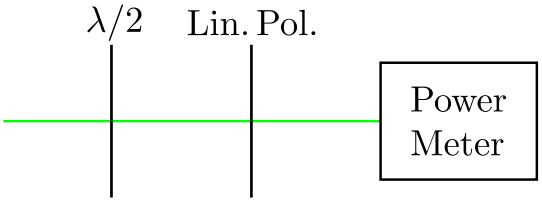

Figure 3.3: A schematic overview of the setup used to calibrate the half waveplate (indicated here with $\lambda/2$)

the Mueller matrices of a waveplate and a linear polarizer, we compute the resulting Stokes vector as function of θ and δ, as shown in Equation 3.3.

$$\frac{1}{2}\begin{pmatrix}1&1&0&0\\1&1&0&0\\0&0&0&0\\0&0&0&0\end{pmatrix}\overline{\mathbf{M}}_{\lambda/n}(\theta)\begin{pmatrix}1\\1\\0\\0\end{pmatrix}=\begin{pmatrix}\frac{1}{2}(1+\cos^2(2\theta)+\cos(\delta)\sin^2(2\theta))\\\frac{1}{2}(1+\cos^2(2\theta)+\cos(\delta)\sin^2(2\theta))\\0\\0\end{pmatrix}. \tag{3.3}$$

We then rotate the waveplate, change θ, and see that the measured power is a sinusoidal function as a function of θ. To this data we fit a sinusoidal function and extrapolate the retardance from the equation

$$\frac{1}{2}(1+\cos^2(2\theta)+\cos(\delta)\sin^2(2\theta)) = p_0\cos(4(\theta'-p_1))+p_2, \tag{3.4}$$

where p_0, p_1, p_2 are the fitparameters and θ' is the angle of the rotation mount. We do not know the exact angle at which the waveplate is placed in the rotation mount and therefore we fit p_1 to find $\theta'-p_1=\theta$. Note that we do not fit the frequency, since we already know its value to be 4. From here on we will denote p_1 by θ_0.

This equation must hold for all values of θ. To solve it, we can thus use a convenient value such as $\theta=\pi/4$. This reduces Equation 3.4 to

$$\frac{1}{2}(1+\cos(\delta)) = -p_0+p_2, \tag{3.5}$$

and therefore we get

$$\delta = \arccos(2(p_2-p_0)-1). \tag{3.6}$$

Even though we use achromatic waveplates for the calibration, the retardance still has a slight wavelength dependence. Therefore we determined the retardance using $\lambda = 570\,\text{nm}, 580\,\text{nm}, 590\,\text{nm}$ and $600\,\text{nm}$. We create Bose-Einstein condensate with $\lambda_{\text{cutoff}} \approx 590\,\text{nm}$. Thus the range in used wavelengths for the calibration extends from above the condensate to below the thermal cloud.

The results for the retardance of the half waveplate and quarter waveplate for $\lambda = 590\,\text{nm}$ are shown in Figure 3.4. For the half waveplate the minimum of the normalized data is close to 0, but there is still a small offset. This is due to the retardance not being equal to 0.5. This contributes to a small amount of of circular light, as described in Section 2.2.2. Consequently the circular light is only filtered out half by the linear polarizer. For the quarter waveplate this effect is much larger as seen in a large offset. We average δ over the four wavelengths. The averaged values are $\delta_{\lambda/2} = 0.515 \pm 0.002$ and $\delta_{\lambda/4} = 0.277 \pm 0.001$ respectively.

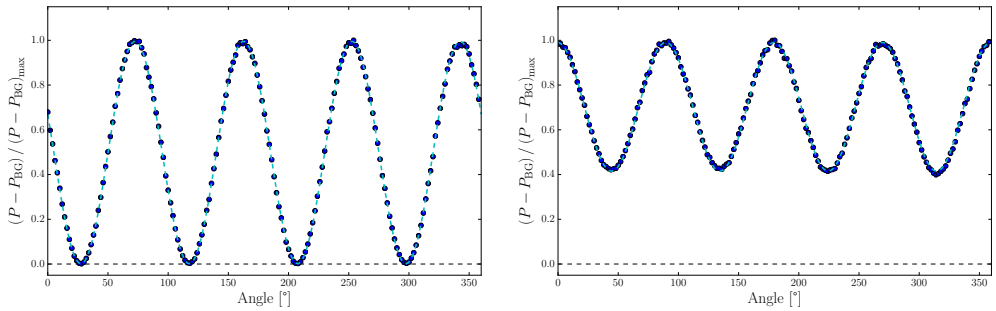

Figure 3.4: Measured normalized power is plotted as a function of the angle of the rotation mount. The dashed line through the data points is a sinusoidal fit. From the phase and offset $\delta_{\lambda/2}$ and θ_0 of the waveplates are determinded. The left panel shows data when the half waveplate is used. The right panel shows the data when the quarter waveplate is used.

Computing matrix elements

We place the half waveplate in front of the polarization setup after the last mirror that directs our light source into the setup. This ensures that the polarization is not changed by reflecting of a mirror. We place the quarter waveplate behind it at an angle of $-45°$. Using Mueller matrices we again compute the resulting Stokes vector as a function of the angle θ of the half waveplate. This Stokes vector we call $\mathbf{S}_{45}(\theta)$ and is shown in Equation 3.7.

$$\begin{aligned}\mathbf{S}_{45}(\theta) = \overline{\mathbf{M}}_{\lambda/2}(\theta) \begin{pmatrix} 1 & 0 & 0 & 0 \\ 0 & \cos(\delta_{\lambda/4}) & 0 & -\sin(\delta_{\lambda/4}) \\ 0 & 0 & 1 & 0 \\ 0 & \sin(\delta_{\lambda/4}) & 0 & \cos(\delta_{\lambda/4}) \end{pmatrix} \begin{pmatrix} 1 \\ 1 \\ 0 \\ 0 \end{pmatrix} = \\ \begin{pmatrix} 1 \\ \sin(\delta_{\lambda/2})\sin(\delta_{\lambda/4})\sin(2\theta) + \cos(\delta_{\lambda/4})\left(\cos^2(2\theta) + \cos(\delta_{\lambda/2})\sin^2(2\theta)\right) \\ \cos(2\theta)\sin(2\theta) - \cos(\delta_{\lambda/2})\cos(2\theta)\sin(2\theta) \\ -\cos(\delta_{\lambda/4})\sin(\delta_{\lambda/2})\sin(2\theta) + \sin(\delta_{\lambda/4})\left(\cos^2(2\theta) + \cos(\delta_{\lambda/2})\sin^2(2\theta)\right) \end{pmatrix},\end{aligned} \tag{3.7}$$

where $\overline{\mathbf{M}}_{\lambda/2}(\theta)$ is the Mueller matrix of the half waveplate. We rotate the half waveplate and measure the response of the polarisation setup on our camera. We

again repeat this for $\lambda = 570\,\text{nm}$, $580\,\text{nm}$, $590\,\text{nm}$ and $600\,\text{nm}$ because the BEC and thermal cloud consist of a range of wavelengths. We can of course also set the quarter waveplate to 0° to get the following Stokes vector $\mathbf{S}_0(\theta)$

$$\mathbf{S}_0(\theta) = \begin{pmatrix} 1 \\ \cos^2(2\theta) + \cos(\delta_{\lambda/2})\sin^2(2\theta) \\ \sin(\delta_{\lambda/2})\sin(\delta_{\lambda/4})\sin(2\theta) + \cos(\delta_{\lambda/4})\left(\cos(2\theta)\sin(2\theta) - \cos(\delta_{\lambda/2})\cos(2\theta)\sin(2\theta)\right) \\ -\cos(\delta_{\lambda/4})\sin(\delta_{\lambda/2})\sin(2\theta) + \sin(\delta_{\lambda/4})\left(\cos(2\theta)\sin(2\theta) - \cos(\delta_{\lambda/2})\cos(2\theta)\sin(2\theta)\right) \end{pmatrix} \tag{3.8}$$

Typical data for both $\mathbf{S}_{45}(\theta)$ and $\mathbf{S}_0(\theta)$ are shown in Figure 3.5. Each panel shows

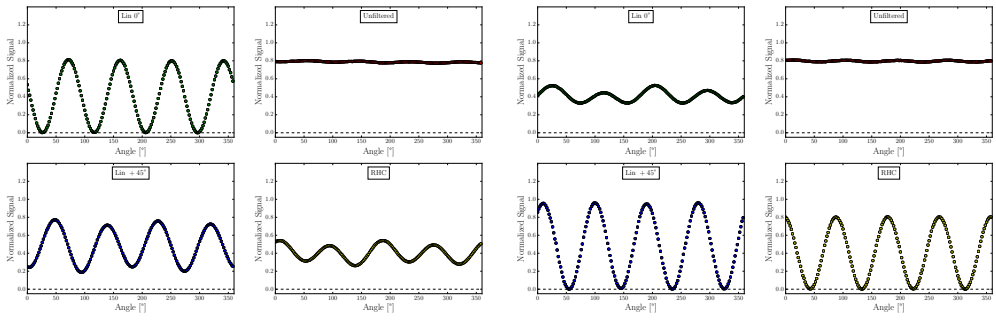

(a) Measured normalised power as a function of the angle of the rotation mount for four different paths as recorder on the Andor Zyla camera. The quarter waveplate is placed at $\theta_{\lambda/4} = 0°$.

(b) Measured normalised power as a function of the angle of the rotation mount for four different paths as recorder on the Andor Zyla camera. The quarter waveplate is placed at $\theta_{\lambda/4} = -45°$.

Figure 3.5: Typical data taken

a different path. The x-axis shows the angle of the rotation mount of half waveplate and the y-axis the power of the respective path as recorded on the Zyla. If the setup would be perfect, the unfiltered path could be used as a direct measurement of the intensity, i.e. S_0. However the signal oscillates due to the slight polarization dependence of the setup, mostly caused by the beam splitter cubes. A different way of looking at this is to say that the off diagonal elements of $\overline{\mathbf{M}}$ are non-zero. In the other panels it can also be seen that the maxima and minima of the signal differ depending on the angle of the rotation mount. This is because the signal is a mixture of different components of $\mathbf{S}_{45}(\theta)$ (or $\mathbf{S}_0(\theta)$).

For each path we can now choose whether to use the data gathered from $\mathbf{S}_{45}(\theta)$ or $\mathbf{S}_0(\theta)$. We choose $\mathbf{S}_0(\theta)$ for the unfiltered and linear 0° path and $\mathbf{S}_{45}(\theta)$ for linear 45° and RHC path. In that way we choose the datasets with the highest amplitudes and our fits are more accurate. This is justified since the fits on the data sets are independent of each other. Each fit corresponds to one row in the matrix. In our fit routine we fix the values of $\delta_{\lambda/2}$ and $\delta_{\lambda/4}$ to the values found in Section 3.2.1. In order to take their error into account we fit 9 times per wavelength where we add

or subtract the error of $\delta_{\lambda/2}$ and $\delta_{\lambda/4}$ in all possible combinations. The results for $\lambda = 600\,\text{nm}$ are shown in Figure 3.6. The fits are plotted as a dashed line.

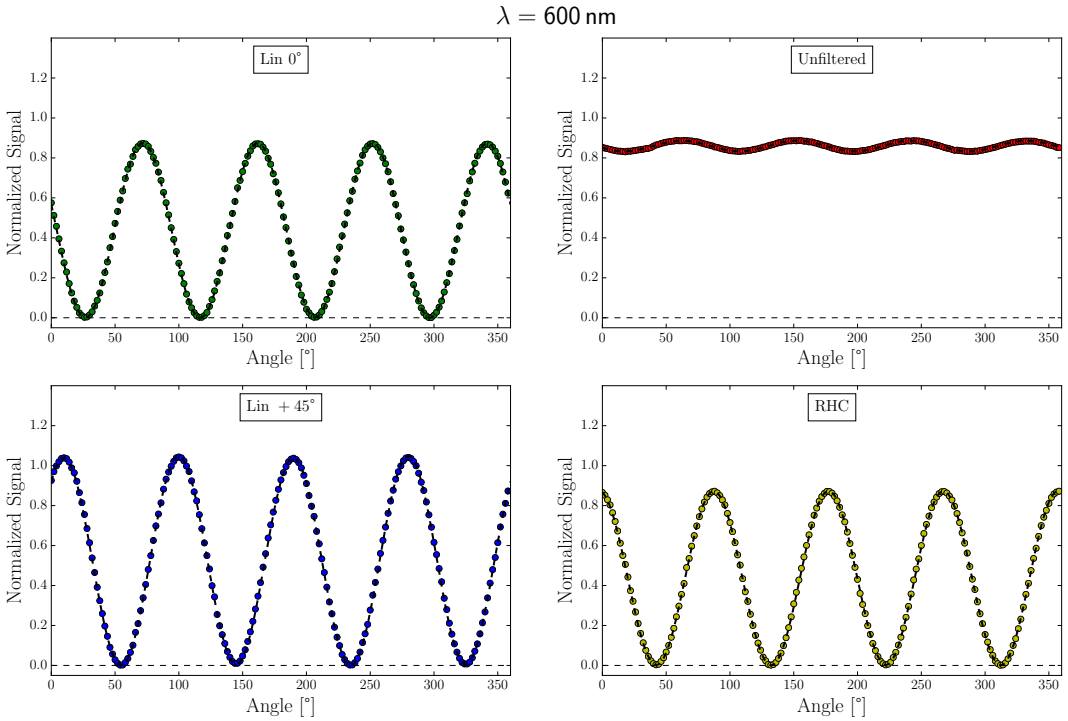

Figure 3.6: Measured normalized power as a function of the angle of the rotation mount for four different paths. The dashed line is the fit to determine the matrix elements of the calibration matrix.

We invert each matrix to get the matrices we wanted to compute. From one camera image we compute multiple Stokes vectors by applying the inverted matrices and then normalize the Stokes vector with respect to S_0. Afterwards we average them to get the final Stokes vector.

Testing the calibration

In order to validate the calibration we sent in light with multiple random, but known, polarization states into our setup for multiple wavelengths. We do this by rotating the half waveplate and quarter waveplate to random angles for each wavelength. From these angles we compute the Stokes vector of this random polarization state. Using the camera image we reconstruct the Stokes vector and we compare the two. The results are shown in Table 3.1. The individual measurements are separated by a horizontal line in the table. For each measurement the top row consist of the known Stokes parameters and the bottom row of the reconstructed ones. The error on the reconstructed Stokes parameters is on average 0.040 ± 0.036. We conclude that the

setup is calibrated and can be used to measure the polarization of the Bose-Einstein condensate.

$\mathbf{S_0}$	$\mathbf{S_1}$	$\mathbf{S_2}$	$\mathbf{S_3}$
1.00	-0.12 ± 0.02	-0.68 ± 0.02	-0.73 ± 0.02
1.00	-0.14 ± 0.02	-0.65 ± 0.04	-0.75 ± 0.03
1.00	0.99 ± 0.01	0.06 ± 0.02	-0.16 ± 0.02
1.00	0.99 ± 0.06	0.02 ± 0.05	-0.12 ± 0.04
1.00	0.55 ± 0.01	-0.36 ± 0.02	-0.75 ± 0.02
1.00	0.55 ± 0.05	-0.37 ± 0.03	-0.75 ± 0.02
1.00	-0.96 ± 0.01	0.04 ± 0.01	-0.28 ± 0.02
1.00	-0.98 ± 0.01	0.09 ± 0.02	-0.25 ± 0.03
1.00	-0.23 ± 0.01	-0.65 ± 0.02	-0.73 ± 0.02
1.00	-0.18 ± 0.02	-0.62 ± 0.04	-0.78 ± 0.03
1.00	-0.82 ± 0.01	0.17 ± 0.01	-0.55 ± 0.02
1.00	-0.82 ± 0.02	0.14 ± 0.02	-0.60 ± 0.04
1.00	0.17 ± 0.01	0.98 ± 0.01	-0.06 ± 0.02
1.00	0.27 ± 0.06	1.08 ± 0.10	-0.22 ± 0.08
1.00	-0.83 ± 0.01	0.56 ± 0.01	0.06 ± 0.02
1.00	-0.85 ± 0.01	0.58 ± 0.06	0.11 ± 0.05
1.00	-0.87 ± 0.01	-0.50 ± 0.01	-0.06 ± 0.02
1.00	-0.88 ± 0.01	-0.45 ± 0.02	-0.15 ± 0.03

Table 3.1: Comparing random Stokes parameters to reconstructed Stokes parameters.

4. Interaction Results

The interaction results contains multiple sections. First we discuss the design of the experiment. After this the analysis is explained. Finally we look at the results.

Experiment design

To investigate the strength of the photon-photon interactions in the condensate we vary the photon density inside the cavity. We vary this by applying a certain voltage to the first AOM, as discussed in Section 3.1. By determining the size of the condensate as function of the condensate photons we obtain a measure for the interaction strength using Eq 2.28. All the images are on a single shot basis. The experiments are performed with a duty cycle of 4.0×10^{-6} with a pulse width of 500 ns. The exposure time of the camera is 1 ms. We perform two experiment using dye concentrations of 1.5 mM and 6.0 mM. The experiments are performed using different gain settings on the camera, as to prevent saturation of the camera.

We vary the photon density by interleaving a positive with a negative power ramp, increasing or decreasing the photon density respectively. Each interleaved power ramp consists of 50 shots. One full experiment consists of 50 interleaved power ramps. By interleaving the power ramps cumulative heating effects of each individual ramp are excluded. If we see growth in the size of the condensate, we can conclude that this is established within one shot. The range of the power ramps are chosen such that it contains powers below and above threshold.

Analysis

The data consists of real colour images taken by the camera (Point Grey Chameleon, CMLN-13S2C-CS). The resolution of the images is found by measuring the diameter of the small cavity mirror in pixels. The found resolution is 1.4 µm/pixel.

The center of the condensate is found by fitting a two-dimensional Gaussian to the image. To be able to compare the spatial profile to Eq 2.25, a radial average is computed for every image. An example of such a radial average is shown in Fig 4.2.

In order to compare the results with the density profile from Equation 2.25, we need to find l_{HO} and Ω. Both depend on q and $\lambda_{\mathrm{cutoff}}$ as discussed in Section 2.1. The

mode number q calculated using Equation 2.21. For a certain cavity distance we measure $\lambda_1 = 622.93\,\text{nm}$ and $\lambda_2 = 596.74\,\text{nm}$. This leads to

$$q = \frac{\lambda_1}{\lambda_1 - \lambda_2} \approx 23. \tag{4.1}$$

Counting back from there we find that we can reach $q = 8$. For the measurements we use $q = 10$. The cutoff wavelength is measured to be $\lambda_{\text{cutoff}} = 592.85\,\text{nm}$.

We rescale the data with l_{HO} and $\hbar\Omega$. To be able to fit the data to the density profile there are two aspects we have to take into account. First is the detection efficiency and second is the growth of the condensate. For both the camera and the dichroic mirror we know the efficiency for each wavelength. From this we can compute a efficiency per cavity mode which we call η_n. Beside η_n there is also an overall detection efficiency, which acts as a scalefactor, I_0. Lastly we assume a constant background consisting of leak light that falls on the camera. This leads to the following intensity profile on the camera

$$I(r) = I_0 \sum_n \frac{g(\varepsilon_n)}{e^{(\varepsilon_n - \mu)/k_B T} - 1} |\psi_n(r)|^2 \, \eta_n. \tag{4.2}$$

We begin by determining I_0. To do this we will determine the temperature and use Equation 2.14 to find the number of photons at threshold. Using this number of photons we obtain a scalefactor which translates the intensity on the camera to the number of photons in the system. To determine the temperature we fit the intensity profile from Equation 4.2 to the radial profiles below threshold where we only see a

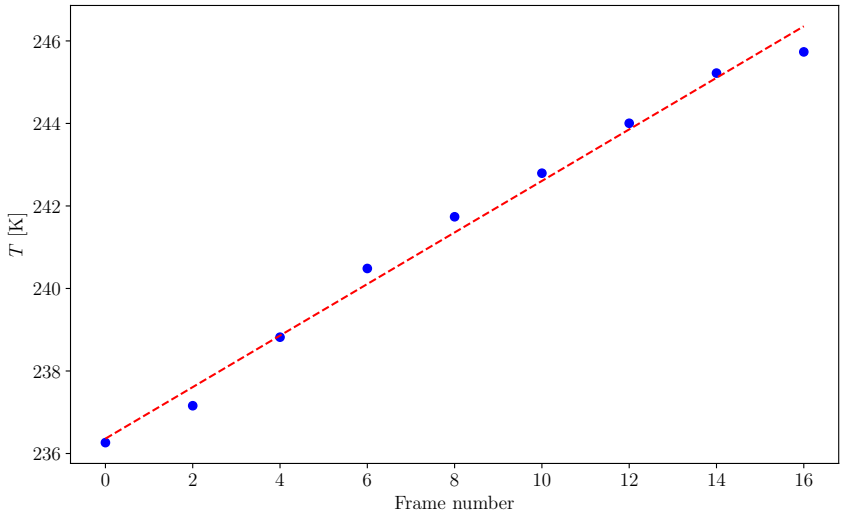

Figure 4.1: Temperature T plotted as a function of frame number for consecutive shots in the positive power ramp. A linear fit to the data point is shown in a red dashed line.

thermal cloud. The used fit parameters are I_0, μ and T. In the vicinity we expect the physical behaviour to be different. Therefore we stay below threshold. From the fits we obtain values of T for different frames which correspond to the positive power ramp. Figure 4.1 shows T plotted as a function of frame number from the positive power ramp.

We see that the temperature increases for larger frame numbers, i.e. higher pump power. As the relation shows to be linear, we fit a linear function to the data points. This fit is shown as the red dashed line. We assume that the increase in temperature below threshold is an extrapolation of this fit. We extrapolate the temperature to find the temperature at threshold. Using Equation 2.14 we find the critical number of photons and consequently I_0.

To measure the growth of the condensate, we define the R_c as the radius of the condensate. We scale the ground state with R_c to take the growth into account. This leads to

$$I(r) = I_0 \left(\frac{g(\varepsilon_0)}{e^{(\varepsilon_0-\mu)/k_BT}-1} |\psi_0(r/R_c)|^2 \eta_n + \sum_{n>0}^{10000} \frac{g(\varepsilon_n)}{e^{(\varepsilon_n-\mu)/k_BT}-1} |\psi_n(r)|^2 \eta_n \right). \tag{4.3}$$

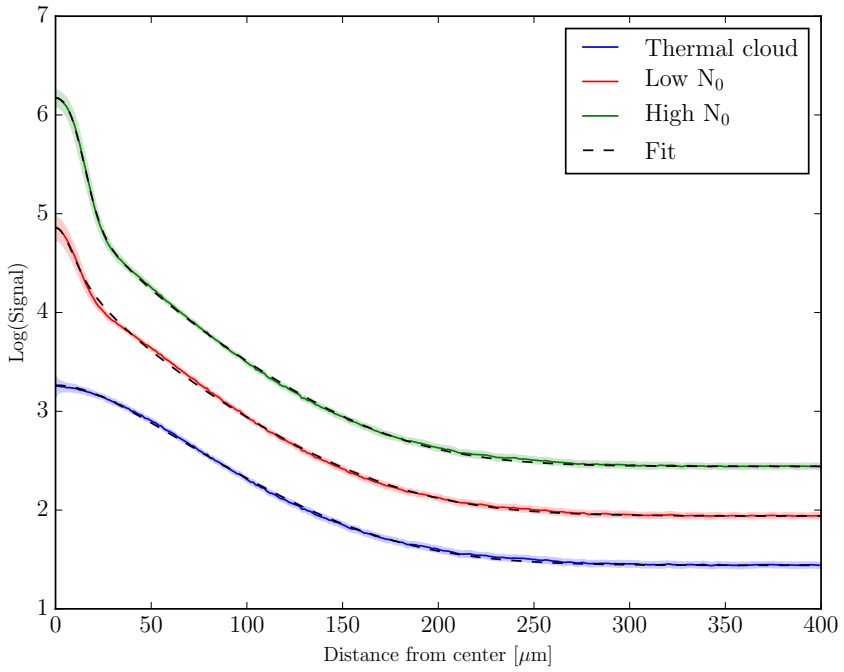

Figure 4.2: Radially averaged profile of the spatial distribution below theshold (blue), low (red) and high (green) number of photons in the condensate N_0. The dashed lines indicate a fit to these radial profiles.

We can now fit the radial averages of the data to this intensity profile. We use μ, T and R_c as fit parameters. Examples of the fit are shown in Figure 4.2. Here the radial profiles are plotted as a functions of the distance from the center r. We fitted a thermal cloud, small condensate and large condensate. The fits are plotted with an artificial offset to see them more clear. The fit is correct for all three radial profiles. We therefore conclude that the fitting procedure works properly.

Positive and negative powerramp

The analysis of the data sets provides the number of photons in the condensate N_0 and the radius of the condensate R_c. The result of this analysis is shown in Figure 4.3. Here, R_c is plotted as a function of N_0 for both the positive (blue circles) and the negative (red circles) power ramp. Note that each data point is averaged over 50 individual spatial distribution gathered from the same number of runs. For increasing N_0, R_c increases i.e. the condensate grows indicating repulsive photon-photon interactions.

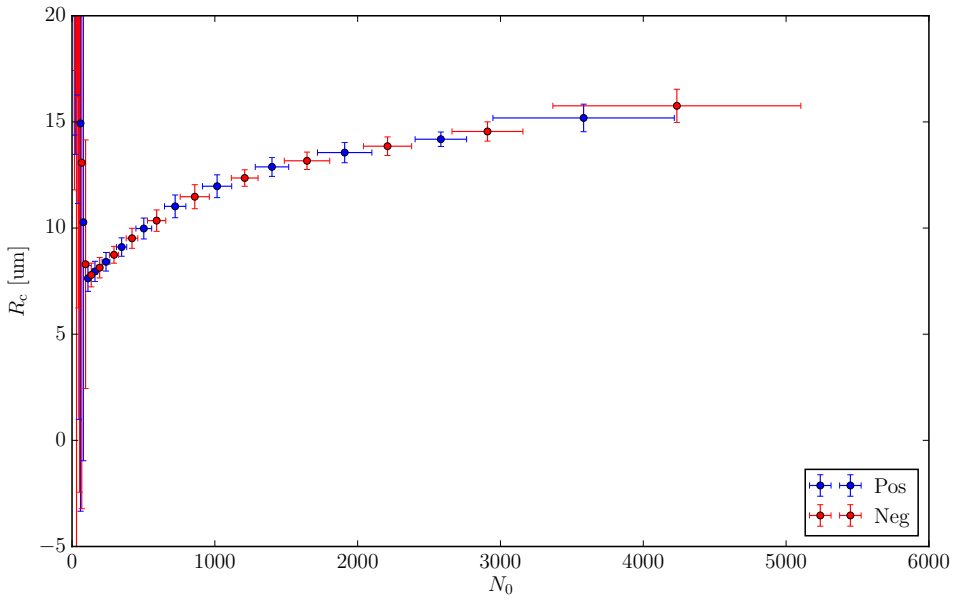

Figure 4.3: Condensate radius R_c plotted as a function of number of condensate photons N_0 for both the positive (blue) and negative (red) power ramp.

For lower values of N_0 variance of the data points diverge. These points originate from the fact that we also apply our fit routine to spatial distribution without a condensate. The radius of the condensate R_c cannot be fitted there and as a result the fit diverges. The diverging points are therefore omitted from the rest of the

analysis. When we pump too hard we excite higher order modes. The frames where we excite higher order modes are also omitted from the rest of the analysis. These frames are selected by visually inspecting the images.

There is no difference between the growth of the condensate for both the positive and the negative power ramp. We conclude that the mechanism that causes the growth takes place within one pump pulse, i.e. 500 ns. Since there is no difference between the positive and negative power ramps, the two are combined into one data set.

Interaction strength

When performing the interleaved power ramp experiment for different dye concentrations we observe that the growth behaviour of the condensate depends on the used dye concentration. In Figure 4.4, R_c is plotted as a function of N_0 for a dye concentration of 1.5 mM (blue) and 1.5 mM (red). We fit Equation 2.28 to the data

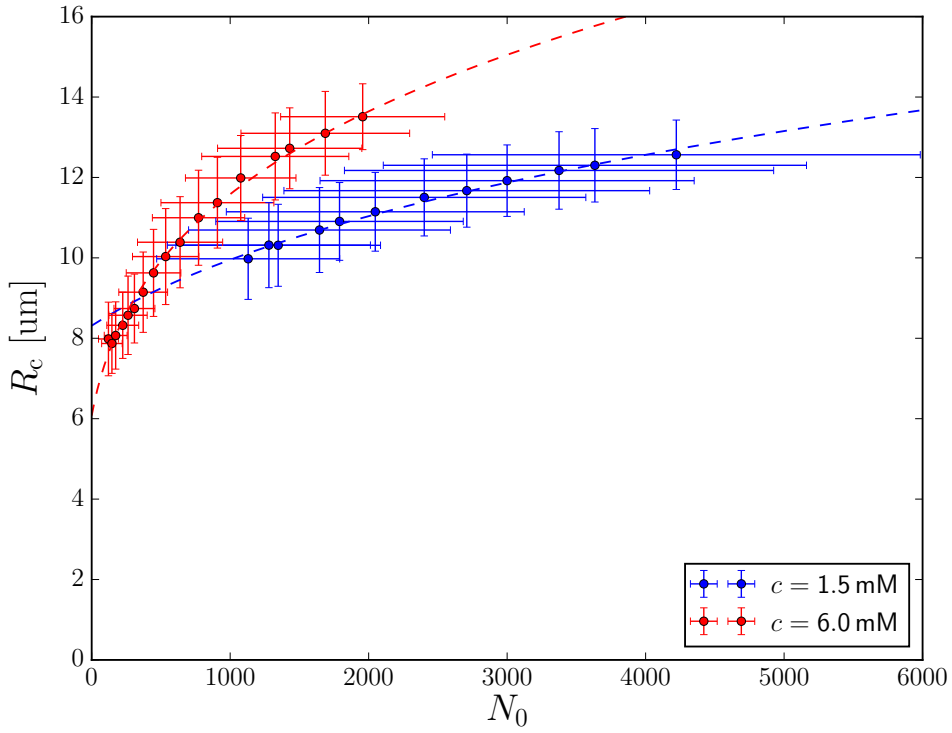

Figure 4.4: Condensate radius R_c plotted as a function of number of condensate photons N_0 for different dye concentration.

using both l_HO and $\tilde{g}$ as fit parameters. The fits are shown as dashed lines. From the fits we obtain $\tilde{g} = (6.6 \pm 0.7) \times 10^{-3}$ and $\tilde{g} = (8 \pm 1) \times 10^{-2}$ when using a dye

concentration of 1.5 mM and 6.0 mM respectively. We expect the values to be much lower, since we assume the interactions to be weak. The values of $\tilde{g}$ however imply strong interactions. The found values of $\tilde{g}$ are strongly dependent on N_0. If the number of condensate photons is determined to be bigger, $\tilde{g}$ will be smaller.

For larger the dye concentration the interaction strength is also larger. We also see that the number of condensate photons that we can reach is different for the two concentrations. This experiment was done using just two dye concentration. It is interesting to know how the interaction strength changes for different dye concentrations. Besides that we know that if the thermal cloud is not visible on the images it has a large impact on N_0. We would therefore also need to validate that the thermal cloud is properly imaged on our camera.

Lastly we need to check if the analysis is consistent. In determining the interaction strength, we also use l_{HO} as a fit parameter. Note that the found value for l_{HO} is different for the two data sets. We can again fit the density distribution to the radial profiles using this value of l_{HO} instead of the one determined with the spectrometer. When repeating this process the value of l_{HO} should converge. Besides that the polarization degeneracy N_s is taken to be 1 because preliminary polarization data suggested that the thermal cloud was polarized. As we will describe in Section 5, this is not the case. Therefore we need to redo this analysis using $N_s = 2$.

5. Polarization Results

The results consist of four sections. First we explain how the data from the camera is analysed and the Stokes parameters are computed. We then discuss the polarization state of the condensate and the thermal cloud and investigate if every newly created condensate has the same polarization state. After which we try to exclude different aspects of the setup to have any influence on the polarization state of the condensate. Lastly, we describe the effect of changing the polarization of the pump beam.

The experiments are performed with a duty cycle of 4.0×10^{-6} with a pulse width of 500 ns. The exposure time of the camera is 1 ms. During previous experiments the large cavity mirror was damaged. We therefore replaced it with a new mirror from CRD Optics. With the new mirror it is harder to reach high condensate fractions. Besides that we saw that we did not image the thermal cloud fully. It turns out that the new mirror is not identical to the old damaged one. We therefore placed back the old damaged mirror and create Bose-Einstein condensates using a part of the mirror that is not damaged. This also provided a visible thermal cloud on the images. For future works another supplier of highly reflecting curved mirrors needs to be found, since the mirrors from CRD Optics are not consistent. Only in the datasets where we use the old damaged mirror, the thermal cloud is properly visible. Due to time limitations, we are not able to reproduce all measurements done with the new mirror, using the old damaged mirror. Consequently, it is stated which mirror is used for which experiment.

Analysis

For every created condensate, the camera (Andor Zyla 5.5) takes two images, one of the photon gas and one background image. On the first image the condensate is imaged four times, one for each path, as described in Section 3.1. We subtract the background and split the image into four seperate cropped images of 400x400 pixels. The result of this is shown in Figure 5.1.

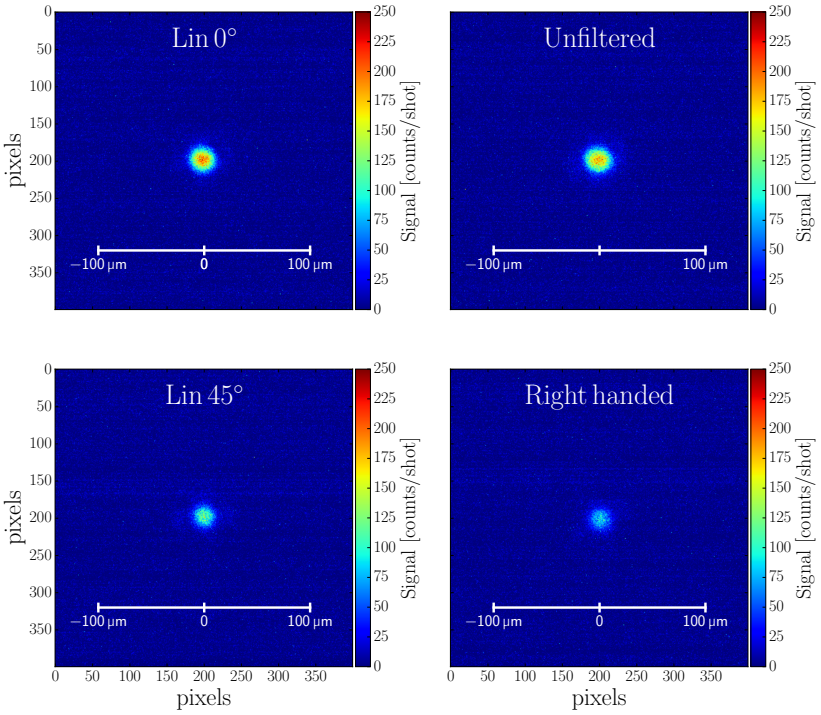

Figure 5.1: An image of a photon BEC as recorded on the Andor Zyla camera.

To determine the Stokes parameters, we need to apply the matrices as described in Section 3.2.1 to every pixel. Therefore it is crucial that we can overlap the four cropped images accurately. The placement of the center of the condensate in each of the four images is determined by fitting a two-dimensional Gaussian to the images. After this the different matrices as described in Section 3.2.1 are applied to the image. Every matrix results in one Stokes vector. These Stokes vectors are averaged to get the final Stokes vector. To make the results more clear a radial average of these Stokes parameters is computed.

In the center of the trap we cannot distinguish between the condensate and the thermal cloud, since the condensate exists on top of the thermal cloud. In the center we measure of mixture of light dominated by the condensate. Moving radially outwards,

the intensity from the condensate lowers and the thermal cloud becomes more visible. For even greater distances the contribution of the condensate is negligible and we only see a thermal cloud.

Measure the polarization

For the first experiment we create a Bose-Einstein condensate using a dye concentration of 1.5 mM, a pump power of P = 1095 mW and we take 100 frames. In this experiment the old damaged mirror is used with $\lambda_{\text{cutoff}} = 592.85\,\text{nm}$. In all the frames the computed Stokes parameters are the same. From this we conclude that every newly created condensate and thermal cloud have the same polarization state. Because of this, we average over all frames. The degree of polarization is computed afterwards using the averaged Stokes parameters as described by Equation 2.39. The error on the degree of polarization is calculated using error-propagation [23]. The other option would be to compute the degree of polarization for every Stokes vector and after the degree of polarization afterwards. The problem would then be that noise around 0 no longer averages out. We therefore first average the Stokes parameters and only afterwards compute the degree of polarization.
The results are shown in Figures 5.2 and 5.3. Figure 5.2 shows 4 panels consisting of the normalized intensity I_0 and three Stokes parameters S_1, S_2 and S_3. The x- and y-axis are in pixels, while the value is denoted by a color scale. Note that we zoom in to be able to see the features better, but can still observe the thermal cloud fully. Figure 5.3 shows the radial averages of the Stokes parameters together with the normalized intensity as a reference. Besides that the degree of polarization is plotted in the fourth panel.

In the two dimensional plots it is difficult to distinguish the thermal cloud, but looking at the normalized intensity in the radial profile, we see it clearly. The condensate extends from the center up to $\sim 20\,\mu\text{m}$. The thermal cloud extends from there up to $\sim 70\,\mu\text{m}$. After this the Stokes parameters diverge, since the signal becomes te low to measure the polarization. Even when measuring the polarization for lower intensities, such as purely the thermal cloud, the variance on the Stokes parameters is larger than for the condensate since the signal to noise ratio for larger distances is smaller.

In the center of the BEC S_1 is 1, while S_2 and S_3 are close to 0. This indicates that the condensate is linearly horizontally polarized. Moving radially outwards it is hard to see what happens to the polarization in the two dimensional plots. In Figure 5.3 it is however clear that S_1 drops for larger distance from the center, while S_2 and S_3 remain around 0.
In Figure 5.2 we see that the condensate is slightly elliptical. The orientation angle ψ is slightly larger than 0. Besides that there are higher order modes visible on the

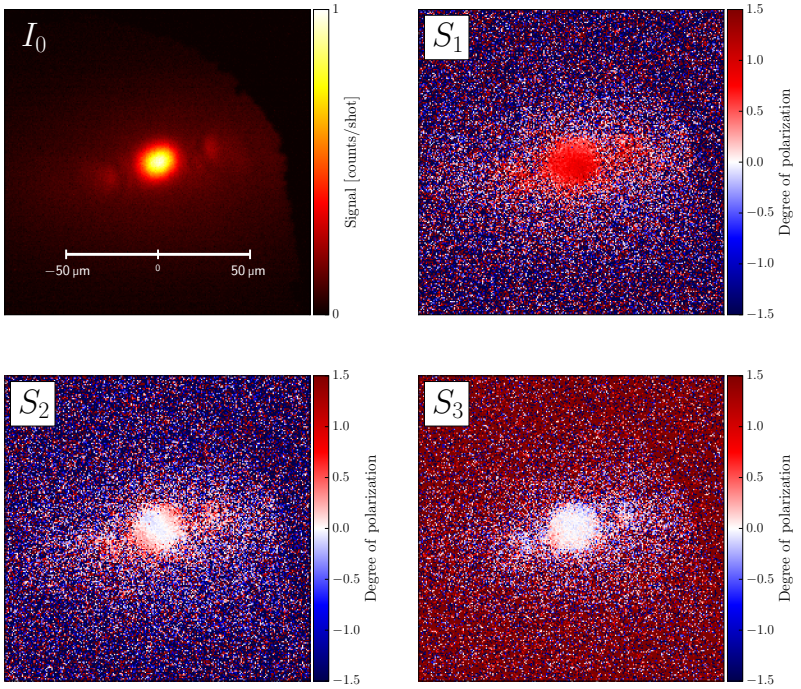

Figure 5.2: 2D Stokes parameters of a photon BEC using a dye concentration of 1.5 mM.

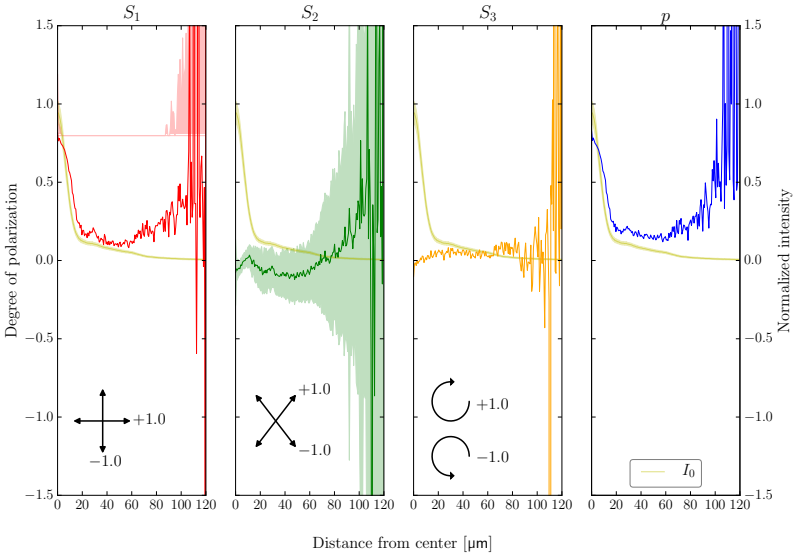

Figure 5.3: Radially averaged Stokes parameters of a photon BEC using a dye concentration of 1.5 mM.

same axis. This indicates that we pump slightly too hard and excite a higher order cavity mode.

From Figure 5.3 we see that the condensate has a degree of polarization close to 1, meaning that is has a well defined polarization state. Moving radially outwards, the degree of polarization drops to close to 0, indicating that the thermal cloud is unpolarized. For even greater distances from the center the degree of polarization diverges, caused by the divergence in de Stokes parameters. The higher order modes are a contributing factor in increasing the degree of polarization slightly above 0. However it is difficult to conclude if the thermal cloud is indeed not polarized from the two-dimensional images. The radial averages are affected by the higher order modes. Therefore we need to redo the measurements without exciting higher order modes in order to measure the polarization state of the thermal cloud. These data imply that the thermal cloud is not polarized, but the higher order modes make this difficult to conclude.

It is remarkable that the polarization state is the same for every newly created condensate, since we would expect the condensate to choose a random polarization state each time it is created, as discussed in Section 2. Based on these result, we expect that there is an aspect in the system that breaks the symmetry.

Possible cause of symmetry breaking

We would like to find the cause of the symmetry breaking. Possible candidates are dye concentration, photon density, a cavity mirror defect, and polarization of the pump beam. In the following sections we describe how these parameters affect the polarization state of the condensate and thermal cloud.

Dye concentration

First we look at the effect of the dye concentration. We repeat the experiment from the previous section using dye concentrations of 6.0 mM and 10.5 mM. The used pump powers are P = 1800 mW and P = 1650 mW respectively. For these data sets the new cavity mirror is used, with $\lambda_{\text{cutoff}} = 591.8\,\text{nm}$. The results for 6.0 mM are shown in Figures 5.4 and 5.5.

From the intensity profile in Figure 5.5 we conclude that the thermal cloud is not visible on the images. This also causes the Stokes parameters to diverge for smaller distances from the center. For that reason it is difficult to conclude anything about the polarization of the thermal cloud based on these data sets. We can however still clearly measure the polarization of the condensate.

The figures again show that in the center S_1 is 1, while S_2 is slighly above 0 and S_3 is close to 0. Moving radially outwards S_1 drops, S_2 flips from slightly above 0 to slightly below and S_3 remains constant. Qualitatively we see the same behaviour as

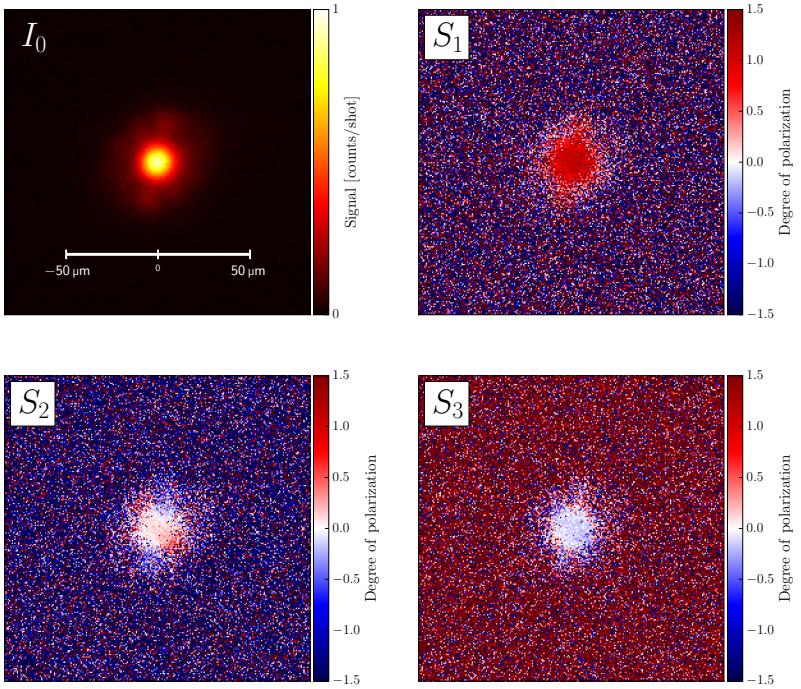

Figure 5.4: 2D Stokes parameters of a photon BEC using a dye concentration of 6.0 mM.

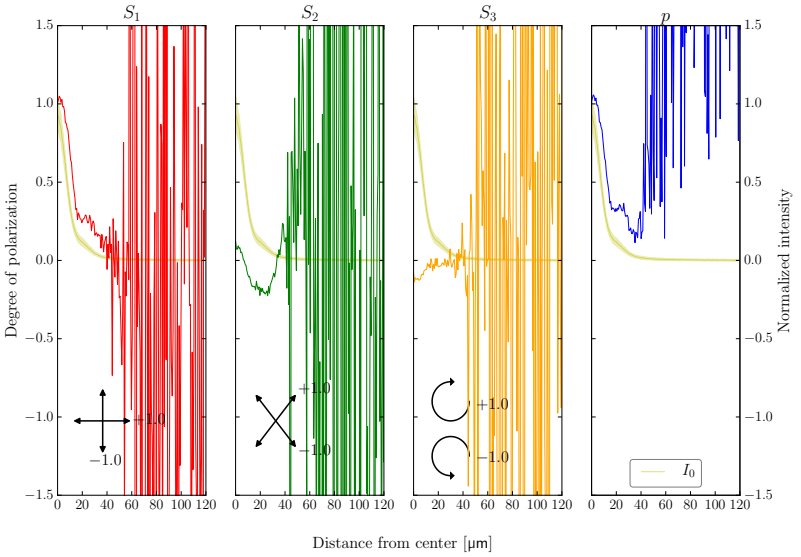

Figure 5.5: Radially averaged Stokes parameters of a photon BEC using a dye concentration of 6.0 mM.

seen when using a dye concentration of 1.5 mM. We conclude that the condensate is still linearly horizontally polarized.
As mentioned before we repeated the experiment for a dye concentration of 10.5 mM.

The results are similar. From this we conclude that the dye concentration does not influence the polarization of the condensate.

Photon density

Secondly we look at the effect of the photon density. We interleave a positive with a negative power ramp as described in Section 4. In this way we can exclude accumulating effects and know that changes in the condensate form within a single shot. We use a pump power of P = 2150 mW, take 100 frames (half in the positive and half in the negative power ramp) and again use a dye concentration of 6.0 mM. The power ramp is created by applying different voltages to the first AOM. We use the new cavity mirror and $\lambda_{\text{cutoff}} = 591.8\,\text{nm}$ We repeat the interleaved power ramp one hundred times and average over the frames with the same pump power in the analysis. The results for a low condensate fraction are shown in Figures 5.6 and 5.7.

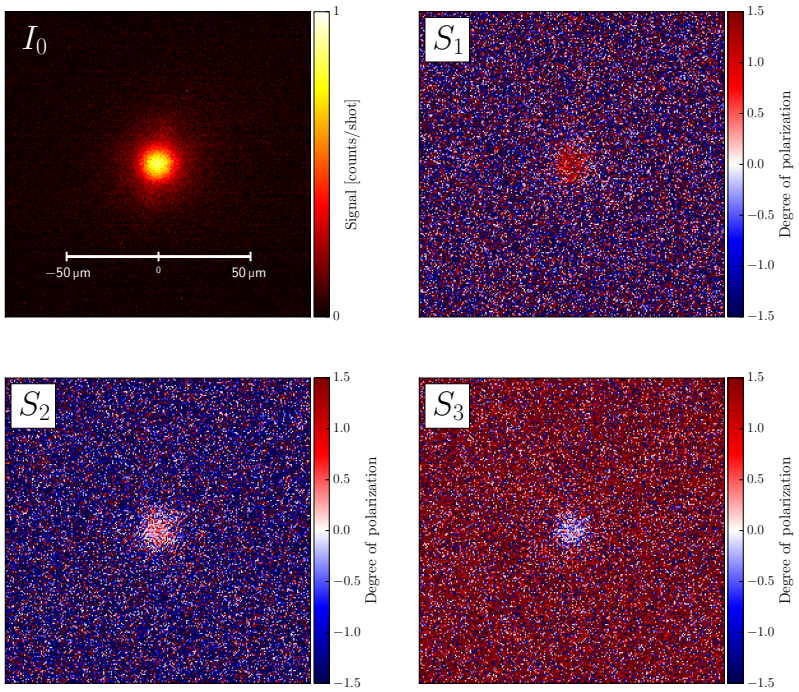

Figure 5.6: 2D Stokes parameters of a photon BEC using a dye concentration of 6.0 mM at lower photon density.

Since the intensity of the captured images is much lower, it becomes hard to distinguish features in the plots. The plots look similar, but the divergence in variance starts at smaller distances from the center. In the center S_1 is 1, S_2 slightly above

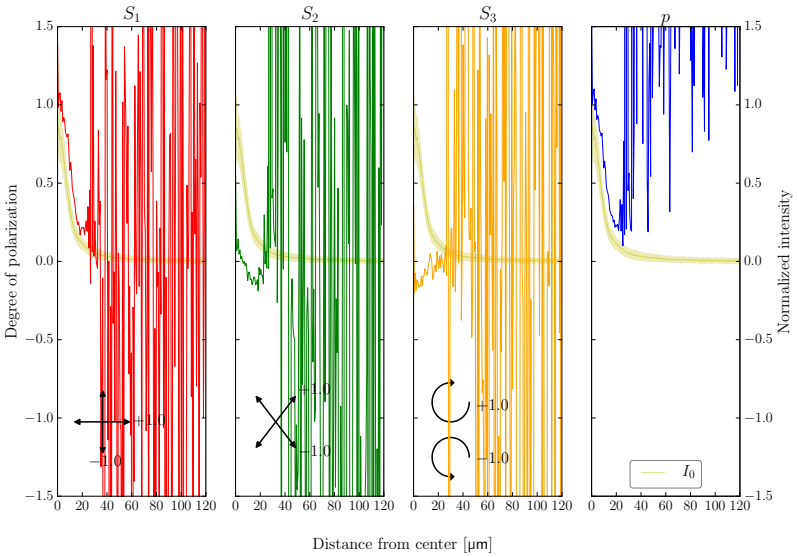

Figure 5.7: Radially averaged Stokes parameters of a photon BEC using a dye concentration of 6.0 mM at lower photon density.

0 and S_3 is close to 0. Moving radially outwards S_1 drops, S_2 flips to slightly below 0 and S_3 remains close to 0. Moving away even further the Stokes parameters diverge. The degree of polarization starts out at 1 and drops when moving radially outwards. It does not drop to 0, as the signal diverges for smaller distances from the center. We repeat the interleaved power ramp for dye concentration of 1.5 mM, 6.0 mM and 10.5 mM. The results are all similar. We conclude that the polarization of the condensate does not depend on dye concentration or photon density.

Cavity mirror

As we mentioned before the fixed polarization must be caused by something that breaks the symmetry in the system. The symmetry of the trap is caused by the curvature of the cavity mirrors. In theory the mirrors that we use have a perfect symmetric curvature, but it could be that the curvature is not perfectly symmetric or that there is a defect on the mirror. This would break the isotropy of the trap. To investigate this, we rotate the large cavity mirror 90° and measure the Stokes parameters of the condensate. The used dye concentration is 1.5 mM and the pump power was kept constant at P = 780 mW. We use the new cavity mirror with $\lambda_{\text{cutoff}} = 591.8\,\text{nm}$. We take 100 frames and average over them. The results are shown in Figures 5.8 and 5.9.

The results are again qualitatively the same. In the center S_1 is equal to 1, while S_2 and S_3 are close to 0. Moving radially outwards S_1 drops, while S_2 and S_3 remain approximately the same. When the intensity gets too low, the Stokes parameters diverge. We again see that the thermal cloud is not visible in this experiment. In the two-dimensional images it can be seen that S_2 and S_2 are not radially symmetric and show symptoms of higher order modes. This can also be seen from the fact that the two-dimensional intensity profile is slightly elliptical. Therefore it is even

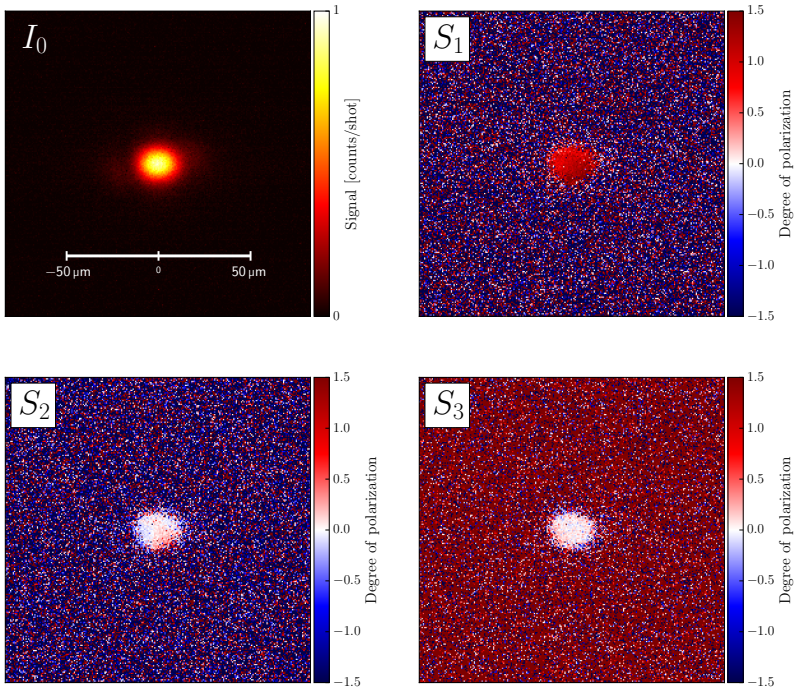

Figure 5.8: 2D Stokes parameters of a photon BEC using a dye concentration of 1.5 mM with the large cavity mirror rotated $\sim 90°$.

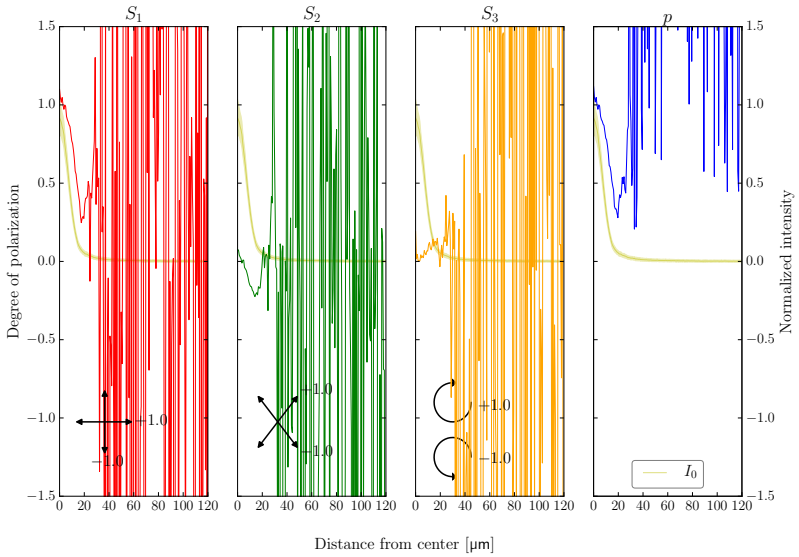

Figure 5.9: Radially averaged Stokes parameters of a photon BEC using a dye concentration of 1.5 mM with the large cavity mirror rotated $\sim 90°$.

more difficult to discuss the Stokes parameters further away from the center. We can however conclude that the condensate is linearly horizontally polarized.

Pump polarization

The polarization of the pump beam is linearly horizontal, which coincides with the polarization of the Bose-Einstein condensate. We therefore investigate if the polarization of the condensate is influenced by changing the polarization of the pump beam. Because of the high angle between the pump beam and the cavity mirror, the dielectric stacking of the mirror acts as a effective polarizer with horizontal transmission. Changing the polarization of the pump beam therefore does not affect the light that is transmitted through the cavity mirror, but only affects the amount of light that is transmitted. One has to be careful when thinking of the cavity mirror as a polarizer with a transmission axis. If it was a polarizer, rotating the mirror would lead to changing the polarization of the light that is transmitted. In our case rotating the mirror does not have this effect since the angle between the pump beam and the dielectric stacking does not change. In order to change the polarization of the light that is transmitted, we need to change the plane of incidence of the pump beam with the cavity mirror. We therefore place a half waveplate and a beam splitter cube after the third AOM. We split the beam path in two and with the half waveplate we regulate the amount of light in each path. The transmitted path is the beam path as discussed earlier. The reflected path is brought up to a different height and is eventually redirected into the cavity, again making a angle of 65°. The plane of

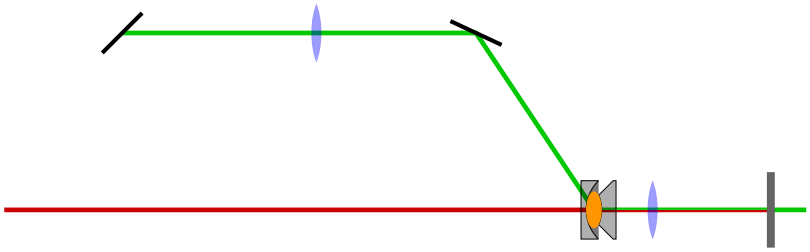

Figure 5.10: A schematic overview of the second pump beam path looking from the side.

incidence is now perpendicular to the table. A schematic overview of how the beam enters the cavity is shown in Figure 5.10.

With this addition to the setup we measure the polarization using a dye concentration of 1.5 mM, constant pump power of $P = 545\,\mathrm{mW}$. The old cavity mirror is used with $\lambda_{\mathrm{cutoff}} = 592.85\,\mathrm{nm}$. We take 100 frames and average over them like before. The results are shown in Figures 5.11 and 5.12.

In Figure 5.11 it is clear that S_1 is now -1 in the center of the trap instead of 1. S_2 and S_3 are still close to 0. This indicates that the condensate is now linearly vertically polarized. Thus we can change the polarization state of the Bose-Einstein conden-

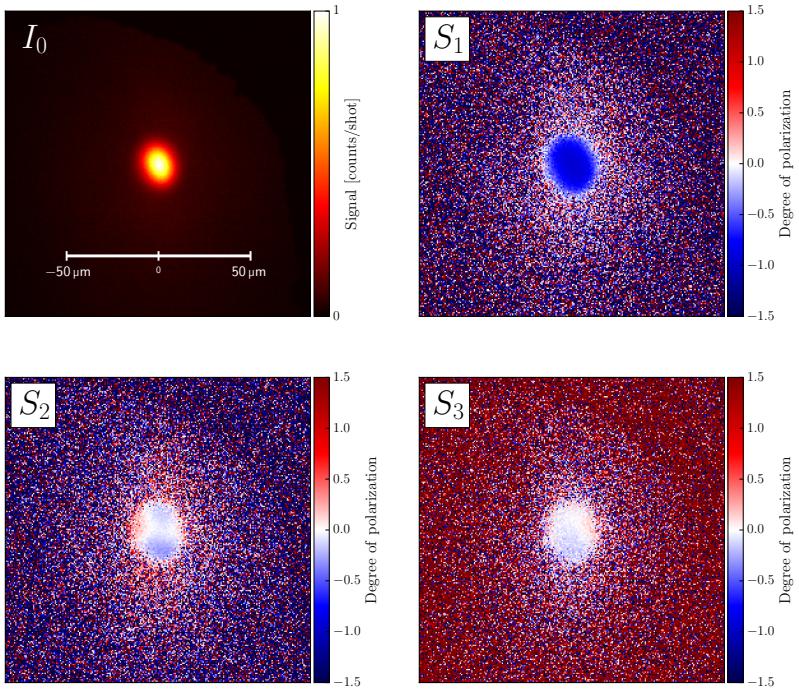

Figure 5.11: 2D Stokes parameters of a photon BEC using a dye concentration of 1.5 mM with plane of incidence perpendicular to the optics table.

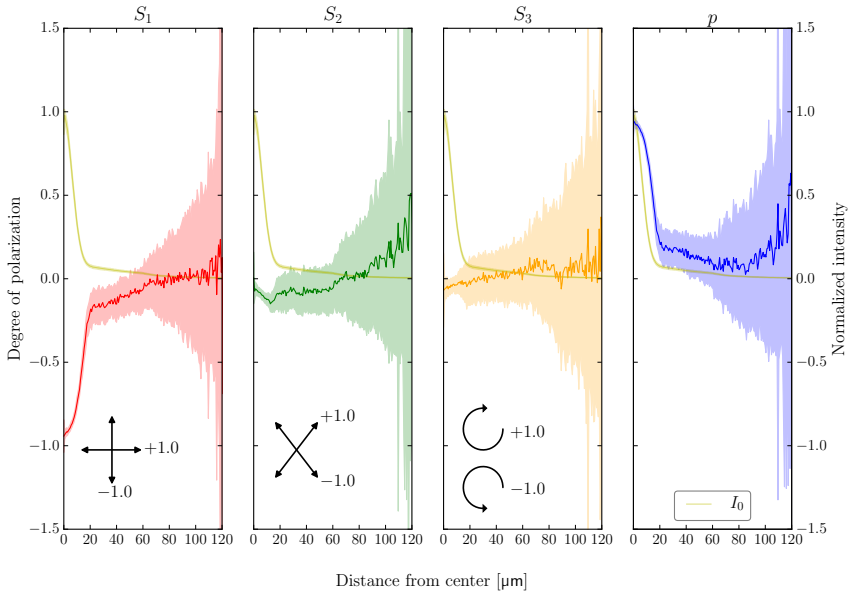

Figure 5.12: Radially averaged Stokes parameters of a photon BEC using a dye concentration of 1.5 mM with plane of incidence perpendicular to the optics table.

sate by changing the intra-cavity polarization of the pump beam. Moving radially outwards it is again hard to distinguish the thermal cloud in the two-dimensional images. We do notice that the condensate is slightly elliptical, but the orientation angle ψ is now slightly larger than 90°.

As a result of the high angle between the pump beam and the cavity mirror, the focus of the pump beam is not circular but elliptical, with its orientation angle corresponding to the plane of incidence. We believe that this causes the higher order modes in the direction where the ellipse is large to be excited first. This can also be seen in the orientation angle of the Bose-Einstein condensate if we pump too hard. When we change the plane of incidence to be perpendicular with the optics table, the orientation angle of the focus rotates by 90°. This also causes the higher order modes to rotate.

In Figure 5.12 we can now again see the thermal cloud extending up to $\sim 70\,\mu$m in the normalized intensity profile. In the radial averages we see that only S_1 changed sign for small distances from the center. Moving radially outwards, S_1 increases to 0, while S_2 and S_3 are close to 0 for a long range. Around 70 µm the Stokes parameters diverge, since there is only background to measure. We conclude that the condensate is linearly vertically polarized. These data also imply that the thermal cloud is unpolarized, but to conclude it we need a measurement without any higher order modes excited.

We can influence the polarization of the Bose-Einstein condensate by changing the

plane of incidence of the pump beam and the cavity. The downside is that with one beam we can only transmit linearly polarized light into the cavity. To be able to see what happens when we pump with circular polarized light, we need two pulses arriving at the same time of which we can accurately control the phase. Getting the pulses to arrive at the same time is simply done by having the different paths have the same length. A difference in length of 1 cm corresponds to only $\sim$ 30 ps time difference. Therefore having the pulses arrive at the same time is experimentally feasible. Controlling the phase is however more challenging.

6. Conclusion and Outlook

In this thesis we described our research into different properties of a two-dimensional Bose-Einstein condensate of photons. We first determined the strength of the photon-photon interactions in the condensate by looking at the growth of the condensate as a function of pump power. This was done by taking single shot images of the condensate for multiple pump powers. The different pump powers were arranged in an interleaved power ramp. The results show that there are no accumulating heating effects. The growth of the condensate is thus established within one shot of 500 ns. We determined the effective interaction strength to be $\tilde{g} = (6.6 \pm 0.7) \times 10^{-3}$ and $\tilde{g} = (8 \pm 1) \times 10^{-2}$ using a dye concentration of 1.5 mM and 6.0 mM respectively. We conclude that the strength of the interactions is dependent on dye concentration and increases for increasing dye concentrations. In order to understand this dependence we need to repeat the experiments for a range of dye concentrations. When performing these experiments we should keep the gain settings of the camera constant. We can then also check if the determination of the scalefactor is consistent for every experiment.

Secondly we took single shot images to determine the polarization state of the Bose-Einstein condensate and the thermal cloud. The polarization state of the condensate or thermal cloud does not change every time a condensate is created. The condensate is linearly horizontally polarized, which coincides with the polarization of the pump beam. The thermal cloud is not polarized. The polarization state of the condensate is independent of dye concentration and pump power. Rotating the cavity mirror along the optical axis also does not influence the polarization state. We showed that the polarization of the condensate is influenced by changing the plane of incidence of the pump.

There are multiple afterthoughts to be had about the experimental setup and the results, which we will discuss here. First of all, for determining the effective interaction strength it is essential that the thermal cloud is imaged properly. The thermal cloud plays an important role in fitting the theoretical model to the radial profile of the Bose-Einstein condensate and thermal cloud. If the outer parts of the thermal cloud are not captured on the camera, the fitting procedure underestimates the spectral temperature and the total number of photons in the system. This leads to an overestimation on the interaction strength. To improve the imaging of the thermal cloud, there are several things that can be done.
Primarily using a camera more sensitive for low photons numbers would improve the imaging of the outer parts of the thermal cloud.
We have also seen that when a too small pump spot is used a proper thermal cloud is not visible. To make sure that the spot is not too small, one should create Bose-

Einstein condensation using a bigger focus and compare the results.
Besides that the imaging of the thermal cloud can be improved by increasing the numerical aperture of the setup. This is now not possible due to the piezo actuators attached to the small cavity mirror. Using smaller pieze elements would counter this problem.
Finally the thermal cloud seems to be elliptical instead of circular. In fact it is the pump spot which is elliptical and visible on the images. Since the analysis uses a radial profile this induces a small error for large enough distance from the center, where the ellipticity becomes visible. The ellipticity of the pump spot is caused by the high angle between the pump beam and the cavity mirror. To negate this one could place prisms on the cavity mirror, as done by the group of Martin Weitz. A different approach could be to create an elliptical pump beam in such a way that it creates a circular pump spot inside the cavity.

Another difficulty of using this setup is that it is hard to know if we excite higher order modes. This is done by looking at taken test images and seeing if the condensate is circular. A big improvement would be to add a accurate spectroscope to the setup. The spectroscope would need to have a very high resolution such that it is able to distinguish between the ground mode and the higher order modes. Using this spectroscope the data quality would improve since we will no longer accidentally excite higher order modes in an experiment.

The effective interaction strength that we found is much larger than expected. One can question the value given the non-interacting nature of photons. Equation 2.28, containing the effective interaction strength, is correct for $\tilde{g}\, N_0/2\,\pi \ll 1$. The values found for $\tilde{g}$ and N_0 do not obey this relation. Therefore it is a good idea to also determine the effective interaction strength using the Thomas-Fermi limit. If the found interaction strength is consistent with the one reported here, it will strengthen the results found in this thesis.

Besides the interaction strength, there are also several continuations to be performed regarding the polarization measurements. Primarily final measurements need to be performed to be able to confirm that the thermal cloud is not polarized.
It would also be interesting to look at the transition from condensate to thermal cloud. We know that the Bose-Einstein condensate lies on top the thermal cloud. In the center of the trap, the condensate dominates the measured polarization. At greater distances from the center it is the thermal cloud that dominates. We can look closer at the transition between these regimes. We can model the total polarization state using the theoretical profiles used to determine the interaction strength. We can therefore spatially determine the contribution in intensity from the condensate and the thermal cloud. It would be interesting to see if their ratio can describe the polarization measured. For this to be possible, we also need to image the thermal cloud fully using the polarization setup.
One aspect that would definitely improve the data quality is to cool the Zyla camera.

When taking the data we were not aware of the ability of the camera to cool the chip. When we now turn on the cooling, the noise is reduced significantly.

Additionally we concluded that the polarization of the light that is transmitted into the cavity is always linear. This means that we need two beams to create circular polarized light. Using this setup we can balance the power in both pump beams. Regulating the phase difference between both beams is unfortunately not possible at this point. We can however guide one of the beams through another AOM. The AOM will cause a small frequency difference between both beams. This will lead to a rapidly changing phase difference between both beams. It is interesting to see how the condensate will react to this.

Furthermore the polarization measurements imply that we need to alter the analysis for the interactions. In the analysis the polarization degeneracy N_s for the thermal cloud and condensate are taken to both be 1. Since the thermal cloud is not polarized, this means that N_s should be 2. The polarization degeneracy of the condensate is however still 1. Therefore we need to redo the analysis and recalculate $\tilde{g}$.

Lastly it would be a good idea to look at the role the dye solvent plays on the polarization. We expect that there is no correlation between the absorbed photon and the emitted photon, because of the many collisions the dye molecule undergoes in the time in between absorption and emission. It could be that this is not the case due to the high viscosity of ethylene glycol. Recent theoretical work describes a polarization dependence on the diffusion of the dye molecules [24]. They show that for low enough angular diffusion constants, the condensate adopts the polarization of the pump beam, which coincides with our results. Replacing the dye solvent by a solvent with lower viscosity could therefore change the measured polarization of the condensate. A candidate for this is methanol. The downside of using methanol however is its high evaporation rate.

In the coming years these improvements can be carried out. This will lead to a better understanding of a Bose-Einstein condensate of photons in a dye-filled microcavity. To even better understand the role the dye, it is promising to look at other thermalizing media, such as semiconductors or quantum dots.

7. Acknowledgements

I would like to thank Dries van Oosten for given me the opportunity to work on the photon Bose-Einstein condensate. I found it an exciting topic to work on and it helped shape my future interest in physics. Your knowledge and understanding of physics is astonishing.
Secondly I would like to thank my daily supervisor Sebastiaan Greveling for his help and for making me feel welcome. You taught me a lot of experimental skills for which I am grateful. Besides that it was just a lot fun working together, while obsessively listening to certain songs. I hope that your career brings you new, fun and challenging experiences.
The other person that helped me in the lab was Javier Hernandez Rueda. Thank you for giving me helpful tips in the lab and for your willingness to discuss problems with our setup.
I would also like to thank Arjon van Lange for having discussions about optics and physics in general, but mostly for creating a lively atmosphere making the coffee breaks very enjoyable.

Without working equipment I would have never been able to finish my master project. Therefore I would like to thank our technicians Cees de Kok, Dante Killian, Frits Diteweg and Paul Jurrius for making time for our many technical requests.

Lastly I would like to thank everyone in the Nanophotonics group for welcoming me, for having interesting discussions about physics, and for the good times had during my time here.

Bibliography

[1] J. Klaers, J. Schmitt, F. Vewinger, and M. Weitz, *Bose-Einstein condensation of photons in an optical microcavity*, Nature **vol. 468**, no. 7323, pp. 545–548 (2010)

[2] K. Perrier, *Photon Bose-Einstein condensation in a dye-filled microcavity*, Master's thesis, Utrecht University (2016)

[3] M. H. Anderson, J. R. Ensher, M. R. Matthews, C. E. Wieman, E. A. Cornell, *et al.*, *Observation of Bose-Einstein condensation in a dilute atomic vapor*, science **vol. 269**, no. 5221, pp. 198–201 (1995)

[4] K. B. Davis, M.-O. Mewes, M. R. Andrews, N. Van Druten, D. Durfee, D. Kurn, and W. Ketterle, *Bose-Einstein condensation in a gas of sodium atoms*, Physical review letters **vol. 75**, no. 22, p. 3969 (1995)

[5] S. N. Bose, *Plancks gesetz und lichtquantenhypothese*, Springer (1924)

[6] A. Einstein and Q. des einatomigen idealen Gases, *Zweite abhandlung*, Sitzber. Kgl. Preuss. Akad. Wiss **vol. 3** (1925)

[7] M. Planck, *On the law of the energy distribution in the normal spectrum*, Ann. Phys **vol. 4**, no. 553, p. 90 (1901)

[8] W. D. Phillips and H. Metcalf, *Laser deceleration of an atomic beam*, Physical Review Letters **vol. 48**, no. 9, p. 596 (1982)

[9] S. Chu, J. Bjorkholm, A. Ashkin, and A. Cable, *Experimental observation of optically trapped atoms*, Physical Review Letters **vol. 57**, no. 3, p. 314 (1986)

[10] C. C. Bradley, C. Sackett, and R. Hulet, *Bose-Einstein condensation of lithium: Observation of limited condensate number*, Physical Review Letters **vol. 78**, no. 6, p. 985 (1997)

[11] S. Jochim, M. Bartenstein, A. Altmeyer, G. Hendl, S. Riedl, C. Chin, J. H. Denschlag, and R. Grimm, *Bose-Einstein condensation of molecules*, Science **vol. 302**, no. 5653, pp. 2101–2103 (2003)

[12] J. Kasprzak, M. Richard, S. Kundermann, A. Baas, P. Jeambrun, J. Keeling, F. Marchetti, M. Szymanska, R. Andre, J. Staehli, *et al.*, *Bose-Einstein condensation of exciton polaritons*, Nature **vol. 443**, no. 7110, p. 409 (2006)

[13] J. Klaers, J. Schmitt, T. Damm, F. Vewinger, and M. Weitz, *Bose-Einstein condensation of paraxial light*, Applied Physics B: Lasers and Optics **vol. 105**, no. 1, pp. 17–33 (2011)

[14] D. J. Griffiths, *Introduction to Quantum Mechanics*, Pearson Education International, 2nd ed. (2015)

[15] C. Pethick and H. Smith, *Bose-Einstein Condensation in Dilute Gases*, Cambridge University Press, 2nd ed. (2008)

[16] S. Hooker and C. Webb, *Laser Physics*, Oxford University Press, 1st ed. (2012)

[17] E. van der Wurff, A.-W. de Leeuw, R. Duine, and H. Stoof, *Interaction effects on number fluctuations in a Bose-Einstein condensate of light*, Physical review letters **vol. 113**, no. 13, p. 135301 (2014)

[18] H. T. Stoof, K. B. Gubbels, and D. B. Dickerscheid, *Ultracold Quantum Fields*, Springer, 1st ed. (2009)

[19] S. Joardar, *Polarimetry* URL `http://www.gmrt.ncra.tifr.res.in/~joardar/lecHtmlPages/lectures/03-Polarimetry.pdf`

[20] S. Akhmanov and S. Nikitin, *Physical Optics*, Oxford University Press, 3rd ed. (2002)

[21] C. U. Keller, *International summer school on solar polarization, lecture 5* URL `http://home.strw.leidenuniv.nl/~keller/Teaching/China_2008/CUK_L05_handout.pdf`

[22] A. W. Khan, *Newton's rings* URL `http://physical-optics.blogspot.nl/2011/06/newtons-rings.html`

[23] J. R. Taylor, *An introduction to Error Analysis*, University Science Books, 1st ed. (1997)

[24] R. I. Moodie, P. Kirton, and J. Keeling, *Polarization dynamics in a photon bec*, arXiv preprint arXiv:1707.01738 (2017)